Title

WD Repeat-containing Protein 5 (WDR5) Localizes to the Midbody and Regulates Abscission*

Journal

Journal of Biological Chemistry, 290(14)

ISSN

0021-9258

Authors

Bailey, Jeffrey K

Fields, Alexander T

Cheng, Kaijian

et al.

Publication Date

2015-04-01

DOI

10.1074/jbc.m114.623611

THE JOURNAL OF BIOLOGICAL CHEMISTRY VOL. 290, NO. 14, pp. 8987–9001, April 3, 2015

WD Repeat-containing Protein 5 (WDR5) Localizes to the Midbody and Regulates Abscission*

Received for publication, November 6, 2014, and in revised form, February 3, 2015 Published, JBC Papers in Press, February 9, 2015, DOI 10.1074/jbc.M114.623611

Jeffrey K. Bailey[‡§], Alexander T. Fields[‡§], Kaijian Cheng[‡§1], Albert Lee[‡§], Eric Wagenaar[‡§], Remy Lagrois[‡§], Bailey Schmidt[‡§], Bin Xia[‡§1], and Dzwokai Ma[‡§2]

From the [‡]Neuroscience Research Institute, [§]Department of Molecular, Cellular, and Developmental Biology, University of California at Santa Barbara, Santa Barbara, California 93106

Background: WDR5 is a protein known for its role in the epigenetic control of gene expression.
Results: During cytokinesis, WDR5 resides at the midbody in the absence of chromatin and promotes normal abscission.
Conclusion: WDR5 is a midbody component and regulates the final steps of cytokinesis.
Significance: WDR5 may have additional functions and binding partners outside of the cell nucleus.

Cytokinesis partitions the cytoplasm of a parent cell into two daughter cells and is essential for the completion of cell division. The final step of cytokinesis in animal cells is abscission, which is a process leading to the physical separation of two daughter cells. Abscission requires membrane traffic and microtubule disassembly at a specific midbody region called the secondary ingression. Here, we report that WD repeat-containing protein 5 (WDR5), a core subunit of COMPASS/MLL family histone H3 lysine 4 methyltransferase (H3K4MT) complexes, resides at the midbody and associates with a subset of midbody regulatory proteins, including PRC1 and CYK4/MKLP1. Knockdown of WDR5 impairs abscission and increases the incidence of multinucleated cells. Further investigation revealed that the abscission delay is primarily due to slower formation of secondary ingressions in WDR5 knockdown cells. Consistent with these defects, midbody microtubules in WDR5 knockdown cells also display enhanced resistance to depolymerization by nocodazole. Recruitment of WDR5 to the midbody dark zone appears to require integrity of the WDR5 central arginine-binding cavity, as mutations that disrupt histone H3 and MLL1 binding to this pocket also abolish the midbody localization of WDR5. Taken together, these data suggest that WDR5 is specifically targeted to the midbody in the absence of chromatin and that it promotes abscission, perhaps by facilitating midbody microtubule disassembly.

Post-translational modifications of histones, including methylation of specific lysine residues of histones H3 and H4, regulate chromatin structure and function by promoting the assembly of protein complexes at specific genomic loci (1, 2). Methylation of histone H3 lysine 4 (H3K4) is enriched within actively transcribed genes and is viewed as a hallmark of transcriptional activity (3–6). In mammals, the COMPASS/MLL family of H3K4 methyltransferases (H3K4MTs) function as a complex consisting of one catalytic subunit (SET1A, SET1B, MLL1, MLL2, MLL3, or MLL4) and four core regulatory subunits (WDR5, RbBP5, ASH2L, and mDPY-30) (1, 7–9). These core regulatory subunits form a subcomplex that dramatically enhances the enzymatic activity of the catalytic subunit, and depletion of any one of the core regulatory subunits leads to a defect in H3K4 methylation (10, 11). The physiological significance of H3K4MTs is highlighted by the fact that translocation of *MLL1* and knock-out of *MLL3* cause cancer in humans and mice, respectively (12). Recently, mutations in MLL2 were found to be the most common cause of Kabuki syndrome (13). In addition, sequencing data from the human cancer genome indicate that several H3K4MT subunits are frequently mutated in a variety of cancers (12).

Although the precise structure of assembled catalytic and core regulatory subunits remains elusive (14–16), WDR5 is essential for the association of RbBP5, ASH2L, and mDPY-30 with MLL1 (11, 15). WDR5 is a highly conserved ~36-kDa protein with a short unstructured N terminus followed by seven WD40 repeats that adopt a seven-bladed β-propeller fold (17). Hierarchical assembly of MLL1 with RbBP5, ASH2L, and mDPY-30 occurs via two distinct binding sites located on opposite faces of the WDR5 β-propeller (15, 18, 19). One site, referred to as the arginine binding cavity, is occupied by the arginine-containing WIN (WDR5-interacting) motif of the MLL/SET catalytic subunit and the other by a motif within the RbBP5 C-terminal tail. Almost all studies of WDR5 have been conducted regarding its nuclear function, and whether this protein has a cytoplasmic role remains unclear. In 2010, Wang *et al.* (20) reported that nuclear WDR5 translocates to the mitochondrial outer membrane where it mediates host response after viral infection. Subsequently, a quantitative proteomics study of SET1/MLL complex stoichiometry identified a large number of novel WDR5-associated proteins, several of which have known cytoplasmic functions (21). These findings suggest that WDR5, like other β-propellers, may function as a scaffolding hub for cytoplasmic signaling modules yet to be identified.

While investigating the role of Golgi-localized mDPY-30 in vesicular transport (22), we observed phenotypes in WDR5-depleted RPE1 (an immortalized nontumor human cell line)

* This work was supported, in whole or in part, by National Institutes of Health Grants 5R21MH086853-02 and 1R21MH086853-01A1 from National Institute of Mental Health (to D. M.).
[1] Present address: Dept. of Pediatrics, West China Second Hospital, Sichuan University, Chengdu, Sichuan Province 610041, China.
[2] To whom correspondence should be addressed: Neuroscience Research Institute, University of California, Santa Barbara, Bldg. 571, Rm. 6129, Santa Barbara, CA 93106. Tel.: 805-893-4745; E-mail: ma@lifesci.ucsb.edu.

and HeLa cells characteristic of cytokinetic defects. Cytokinesis, the final step of cell division that results in two separated daughter cells, is critical for preserving genomic integrity (23–26). Failure of cytokinesis can cause tetra- and polyploidization, a state of chromosomal instability that is thought to precede cancer formation (27, 28). Mechanistically, cytokinesis in animal cells can be divided into two stages, cleavage furrow ingression and abscission (24–26, 29). Upon completion of cleavage furrow ingression, the actomyosin ring is converted to the midbody ring, and the midbody matures to a thickness of ~1–2 μm. Three groups of proteins are essential for the formation of midbody microtubules as follows: (*a*) PRC1-KIF4 (an antiparallel microtubule cross-linker and a PRC1-interacting kinesin, respectively); (*b*) the central spindlin complex MKLP1-CYK4 (an antiparallel microtubule-bundling complex); and (*c*) the chromosomal passenger complex consisting of Aurora B kinase and three additional regulatory subunits (a modulator of MKLP1-CYK4) (30, 31). Although these proteins exhibit dynamic localization during midbody maturation, each group localizes to specific regions of the mature midbody as follows: the dark zone (PRC1-KIF4); the ring (MKLP1-CYK4); and the flanking region (chromosomal passenger complex) (32).

Following maturation of the midbody, cytokinesis enters its second stage, abscission, resulting in the final separation of the two daughter cells (24, 25). During abscission, MKLP1-CYK4 recruits CEP55 to the midbody ring. CEP55 then binds ESCRTIII targeting factors (ALIX and TSG101), which in turn localize ESCRTIII to the ring. Shortly before the final cut, ESCRTIII migrates to an adjacent site known as the secondary ingression where it will mediate membrane fission. The secondary ingression is characterized by the further narrowing of the intercellular bridge from ~1–2 μm to ~ 100 nm (33, 34), and its formation requires the temporal and spatial orchestration of vesicular transport/membrane fusion and clearance of F-actin and microtubules. Although spastin, an ESCRTIII-associated microtubule-severing enzyme (35, 36), has long been postulated to mediate microtubule disassembly at the secondary ingression, a recent study shows that the formation of secondary ingressions does not depend on ESCRTIII (37). Furthermore, additional microtubule disassembly mechanisms have been observed within the midbody (37, 38), and whether spastin is involved in these processes is unknown.

Here, we provide evidence suggesting that the H3K4MT core regulatory subunit WDR5 localizes to the center of midbody in tumor (HeLa) and nontumor (RPE1) cell lines. In particular, the central arginine binding cavity of WDR5 appears to be required for this targeting. Depletion of WDR5 increases the incidence of multinucleated cells, a hallmark of cytokinesis failure. Live cell imaging revealed that midbody abscission is delayed in WDR5-depleted cells and that this phenotype could be largely attributed to slower formation of secondary ingressions. Because the midbody microtubules in WDR5-depleted cells display enhanced resistance to depolymerization by nocodazole compared with control cells, knockdown of WDR5 may cause the abscission defects by enhancing midbody microtubule stability. In its entirety, our data reveal a novel subcellular pool of WDR5 localized to the midbody and support a model in which WDR5 promotes abscission, possibly by facilitating midbody microtubule disassembly.

EXPERIMENTAL PROCEDURES

Reagents—Unless otherwise specified, all reagents/materials were purchased from Fisher Scientific, VWR, Sigma, Life Technologies, or Clontech.

Antibodies—All antibodies used for Western blot analysis (WB),[3] immunocytochemistry (ICC), and immunoprecipitation (IP) are as follows: rabbit anti-ALIX (Santa Cruz Biotechnology sc-271975, WB 1:500); rabbit anti-Aurora B (Abiocode R0117-1, WB 1:2000); mouse anti-centriolin (Santa Cruz Biotechnology sc-365521, WB 1:500); rabbit anti-CEP55 (Santa Cruz Biotechnology sc-134622, WB 1:1000); rabbit anti-CHMP1B (gift from W. I. Sundquist UT592 (39), WB 1:500); mouse anti-CYK4 (Santa Cruz Biotechnology sc-271110, WB 1:1250); rabbit anti-ECT2 (Santa Cruz Biotechnology sc-1005, WB 1:600); mouse anti-GAPDH (Biochain Institute Y3322GAPDH, WB 1:6000); mouse anti-GFP (Roche Applied Science, catalog no. 11814460001, WB 1:1600); rabbit anti-histone H3 (Cell Signaling Technology catalog no. 2650, WB 1:4000); rabbit anti-KIF4A (Bethyl A301-074A, WB 1:2500); rabbit anti-mDPY-30 (Ma Laboratory previously characterized (22), WB 0.25 μg/ml); rabbit anti-MKLP1 (Santa Cruz Biotechnology sc-867, WB 1:1000); goat anti-mouse IgG (Thermo Scientific, DyLight 680 catalog no. 35518, WB 1:6000); goat anti-mouse IgG (Jackson ImmunoResearch, Alexa Fluor 488 catalog no. 115-545-062, Rhodamine Red-X catalog no. 115-295-062, and cyanine Cy5 catalog no. 115-175-146, ICC 1:200); goat anti-rabbit IgG (Jackson ImmunoResearch, Alexa Fluor 488 catalog no. 111-545-144 and Rhodamine Red-X catalog no. 111-295-144, ICC 1:200); rabbit IgG (Invitrogen catalog no. 02-6102, IP 4 μg/ml); goat anti-rabbit IgG (Thermo Scientific, DyLight 680 catalog no. 35568, WB 1:6000); rabbit anti-PRC1 (Santa Cruz Biotechnology sc-8356, WB 1:1000); rabbit anti-RbBP5 (Bethyl A300-107A, WB 1:2000); rabbit anti-TSG101 (Epitomics catalog no. 5347-1, WB 1:2500); mouse anti-α-tubulin (Covance MMS-407R, ICC 1:6000); mouse anti-acetylated-α-tubulin (Santa Cruz Biotechnology sc-23950, ICC 1:1000); rabbit anti-β-tubulin (Santa Cruz Biotechnology sc-9104, WB 1:200); rabbit anti-WDR5 (Bethyl A302-429A, IP 4 μg/ml); and rabbit anti-WDR5 (Bethyl A302-430A, WB 1:3500).

shRNA Expression Constructs—All shRNA constructs were purchased from Sigma as glycerol stocks (pLKO.1-puro vector). Lentiviral particles were generated from shRNA constructs as described below. Target sequences for shRNAs are as follows: control shRNA (SHC002, nontargeting in human or mouse, 5′-CAACAAGATGAAGAGCACCAA-3′); WDR5 shRNA 1 (TRCN0000118047, 5′-GCCTCCTCTCTGAAGATGATT-3′); and WDR5 shRNA 2 (TRCN0000118050, 5′-CCAACCTTATTGTCTCAGGAT-3′).

DNA Expression Constructs—For pLVXpuro and pLNCX constructs, lentiviral particles were generated as described

[3] The abbreviations used are: WB, Western blot; EGFP, enhanced GFP; IP, immunoprecipitation; ICC, immunocytochemistry; MudPIT, multidimensional protein identification technology; ANOVA, analysis of variance; HSD, Tukey's Honestly Significant Difference test.

below. Human and mouse WDR5 cDNAs code for identical amino acid sequences. Subcloning details are as follows: pLVXpuro-EGFP (Clontech, 5′ SmaI, 3′ XbaI); pLVXpuro-WDR5-EGFP (Clontech, 5′XhoI/Klenow, 3′ Bsp1407I, from mouse cDNA, C-terminal EGFP); pLVXpuro-mWDR5-HAC (Clontech, 5′ BamHI, 3′ XbaI/Klenow, from mouse cDNA, C-terminal HA); pEGFP-C3-WDR5_71-173 (Clontech, 5′ XhoI, 3′ SmaI, from mouse cDNA, N-terminal EGFP); pEGFP-C2-EGFP-WDR5 (Clontech, 5′ EcoRI, 3′ BamHI, from mouse cDNA, N-terminal EGFP); pEGFP-C3-EGFP-WDR5-S91K (Clontech, 5′BglII, 3′ EcoRI, subcloned from pHisParallel, gift of M. Cosgrove, N-terminal EGFP); pEGFP-C3-EGFP-WDR5-F133A (Clontech, 5′BglII, 3′ EcoRI, subcloned from pHisParallel, gift of M. Cosgrove, N-terminal EGFP); pLNCX-mCherry (Clontech, 5′ BamHI/Klenow, 3′ HindIII); pLNCX-mCherry-α-Tubulin (Clontech, 5′ NruI, 3′ HindIII, from Addgene plasmid catalog no. 21043, N-terminal mCherry).

Cells—CD8-CIMPR-expressing HeLa (HeLa) (22), hTERT RPE-1 (RPE1, gift from L. Johnson, NRI, University of California at Santa Barbara), and HEK293T cells were cultured in Advanced DMEM (Hyclone DMEM-RS) supplemented with 5% fetal bovine serum, 2 mM glutamine (Life Technologies), and 1× penicillin/streptomycin (Life Technologies). Stably transduced cell lines were grown in the same media with additional supplementation as follows: pLVXpuro and pLKO.1puro (3 μg/ml puromycin); pLNCX (400 μg/ml G418); hTERT (200 μg/ml hygromycin). Cells were dissociated for passage using TrypLE dissociation reagent (Life Technologies). For immunocytochemistry, glass coverslips were coated with 1:500 Matrigel (BD Biosciences) in serum-free medium overnight in a 37 °C incubator and rinsed with 1× PBS before use.

Production of Lentiviral Particles—Production of lentiviral particles and infection of HeLa and RPE1 cell lines were performed as described previously (40). HEK293T cells were grown to 70% confluence in 100-mm plates, and the spent medium was replaced with fresh medium 2 h before transfection. In a sterile transformation tube pMD2.G (2.9 μg), psPAX2 (5.4 μg), and either pLVXpuro, pLKO.1puro, or pLNCX vector containing the appropriate insert (8.3 μg) were mixed. The following components were then added in the following order: 242 μl of 0.1× TE (1 mM Tris, 0.1 mM EDTA, pH 8.8), 128 μl of sterile water, and 41.5 μl of 2.5 M calcium chloride. After brief mixing, 481 μl of 2× HBS (280 mM NaCl, 100 mM HEPES, 1.5 mM Na_2HPO_4, $7.11 \leq pH \leq 7.13$) was added dropwise under gentle vortexing and was incubated for 5 min. After incubation, 830 μl of this transfection mixture was added dropwise to the cells, and medium was replaced 14–16 h post-transfection. Supernatant-containing viral particles was harvested three times, once every 12 h, and pooled supernatants were kept at 4 °C over the collection period. After the last collection, the supernatant was centrifuged for 5 min at 1500 rpm, filtered with a 0.22-μm filter, and stored in aliquots at −80 °C.

Viral Infection and Antibiotic Selection—HeLa or RPE1 cells were trypsinized and re-plated at 60–80% confluence in media containing 10 μg/ml Polybrene (Calbiochem). After cell re-attachment (1–3 h), the medium was removed to a separate well and replaced with viral supernatant. Cells were incubated for 30–60 min before Polybrene-containing medium was added back, and the cells were grown overnight. Approximately 24 h post-transfection, the medium was replaced, and antibiotic selection began at 48 h post-transfection. Transduced cell lines were grown under antibiotic selection for at least 7 days before starting experiments or making frozen stocks.

Isolation and Propagation of Clonal Stable Lines—HeLa cells were infected with lentiviral particles, selected using the appropriate antibiotic, and isolated by limiting dilution into 48-well plates at both low (0.75 cells/well) and high (3 cells/well) cell concentrations. One week after seeding, each well was examined for the presence of single cell colonies, and wells containing more than one colony were excluded. Colonies received half-media changes every 2–3 days and were expanded sequentially from 48-well to 12- and 6-well and T75 culture vessels. Effective knockdown of the target protein was assessed by SDS-PAGE and Western blotting.

Immunoprecipitation—HeLa or RPE1 cells stably expressing WDR5-EGFP were lysed in ice-cold Nonidet P-40 buffer (50 mM Tris-HCl, pH 8.0, 150 mM NaCl, 1 mM EDTA, and 1% Nonidet P-40), with 1× Halt Protease and Phosphatase Inhibitor Mixture (Thermo Scientific) and 1 mM PMSF added just before lysis. Lysates were rocked at 4 °C and cleared by 4 °C centrifugation at maximum speed, and the total protein concentration of the supernatant was normalized across samples using the CB-X protein assay kit (G-Biosciences). Adjusted lysates were bound to a mouse monoclonal anti-GFP antibody covalently conjugated to magnetic microbeads while rocking at 4 °C for 3 h (μMACS GFP-tagged protein isolation kit, Miltenyi Biotec). The beads were washed on μMACS columns with Nonidet P-40 lysis buffer and eluted according to the manufacturer's instructions. HeLa or RPE1 cells stably expressing EGFP alone were included as a negative control.

Midbody and Spindle/Midbody Isolation and Immunoprecipitation—Midbodies were isolated from thymidine/nocodazole-synchronized HeLa cells as described previously by Skop *et al.* (41). Briefly, cells undergoing synchronous cytokinesis were pelleted, resuspended in spindle isolation buffer (2 mM PIPES, pH 6.9, 0.25% Triton X-100, and 20 μg/ml Taxol, 1× Halt mixture protease inhibitor, 1 mM PMSF) and divided into 2 aliquots of equal volume. Pellets, which contain both mitotic spindles and midbodies, were obtained by centrifugation of each aliquot. The total nonspindle/midbody supernatant was collected and mixed with SDS-PAGE sample buffer. To obtain the spindle fraction, one spindle/midbody pellet was resuspended in SDS-PAGE sample buffer (at half of the total supernatant volume). The other spindle/midbody pellet was chilled on ice, washed, and resuspended in 50 mM MES, pH 6.3, and subjected to centrifugation through a cushion of 40% glycerol, yielding isolated midbodies. The isolated midbody pellet was combined with SDS-PAGE sample buffer (again at half of the total supernatant volume). To generate a "non-midbody" fraction for immunoblotting, equal volumes of nonspindle/midbody supernatant and spindle fractions were combined. This was electrophoresed alongside the isolated midbody fraction at a ratio of 2:1 to maintain equal cell numbers in each lane.

For immunoprecipitation from the spindle fraction, the spindle/midbody pellet was resuspended in ice-cold RIPA buffer and incubated with primary antibody (or an equivalent amount

of rabbit IgG as a negative control) for 3 h followed by protein A-Sepharose (Invitrogen) for 2 h at 4 °C. The Sepharose beads were washed four times in ice-cold lysis buffer, and bound proteins were eluted with SDS-PAGE sample buffer at 95 °C for 15 min.

SDS-PAGE and Western Blotting—Cells were lysed in ice-cold RIPA buffer (50 mM Tris-HCl, pH 8.0, 150 mM NaCl, 1 mM EDTA, 1% Nonidet P-40, 0.5% sodium deoxycholate, and 0.1% SDS), with 1× Halt Protease and Phosphatase Inhibitor Mixture (Thermo Scientific) and 1 mM PMSF added as above. After rocking and clearing lysates at 4 °C, the total protein concentration was quantified using the CB-X protein assay (G-Biosciences) and denatured in SDS loading buffer. An equal amount of total protein per lane was loaded into a polyacrylamide gel (6–15%, depending on the proteins to be resolved), and samples were separated by SDS-PAGE and transferred to Immobilon 0.45-μm PVDF membranes (Millipore) using an Owl HEP-1 semi-dry electroblotting system (Thermo Scientific). Membranes were incubated overnight at 4 °C with the appropriate primary antibody diluted in a 1:1 mixture of Odyssey blocking buffer (LI-COR Biosciences) and PBST (1× PBS supplemented with 0.1% Tween 20). Membranes were washed with PBST (three times for 10 min each), incubated in the dark for 45 min with the appropriate secondary antibody (goat anti-mouse or anti-rabbit IgG (H+L) DyLight 680 conjugated, Thermo Scientific), washed with PBST (three times, 5 min each), followed by PBS for 5 min, and dried in the dark. Fluorescence imaging and quantification was performed on an Odyssey Infrared Imaging System (LI-COR Biosciences).

Immunofluorescence—Cells were fixed in 3% UltraPure EM-grade formaldehyde (Polysciences Inc.) for 10 min, quenched with PBS containing 100 mM glycine (two times, 5 min each), and permeabilized with PBS containing either 0.1% saponin or 0.1% Triton X-100 for 15 min. Fixed cells were blocked in buffer (BLOK casein in PBS (G-Biosciences) containing 0.1% saponin and 5% goat serum) for 30 min, incubated with primary antibody diluted in blocking buffer for 2 h, washed in PBS (three times, 5 min each), incubated in fluorophore-conjugated secondary antibody diluted in blocking buffer for 1 h, washed in PBS (three times, 5 min each), incubated in PBS containing 1 μg/ml DAPI for 5 min, and washed in PBS (three times, 5 min each). Coverslips were then allowed to air dry and mounted in PPD antifade (90% glycerol, 10% PBS, 1 mg/ml *p*-phenylenediamine, pH 8.0).

Fluorescence Microscopy—Slides were imaged on an Olympus IX-81 fluorescent microscope using a Plan-Apochromat 60× oil total internal reflection fluorescence objective (Olympus, NA = 1.45), a 1.6× tube factor, Semrock excitation and emission filters, and an X-Cite Exacte illumination source (Lumen Dynamics). Images were captured using a monochrome digital camera (Evolution QEi, Media Cybernetics) controlled with *In Vivo* acquisition software version 3.2.0 (Media Cybernetics). Image analysis was performed using ImageJ (National Institutes of Health), Photoshop, and Illustrator (Adobe).

Live Cell Fluorescence Microscopy—Clonal HeLa cell lines expressing WDR5 shRNAs were transduced with mCherry-tubulin, grown on Matrigel-coated (1:500) glass-bottomed Delta T dishes (Bioptechs), and imaged using an Olympus IX-81 as described above. Because the timing of cytokinesis can vary significantly depending on surface coating conditions and cell density (42), these two variables were controlled as tightly as possible between individual experiments. All live cell imaging experiments were performed at 37 °C using a Delta T Open Dish System equipped with a heated lid and 5% CO_2 perfusion (Bioptechs). For measurements of abscission duration, a 5-image z-series (1.5 μm steps) was acquired at 15-min intervals between anaphase initiation and midbody formation, and at 30-min intervals between midbody formation and abscission. To minimize the potential for phototoxicity, lamp power was set at 10% of maximum, and each exposure was kept <200 ms. For nocodazole treatment, cells were imaged as above, except that treatment with nocodazole in a small volume of prewarmed media (final dish concentration, 10 μM) was initiated upon midbody formation. The nocodazole concentration was chosen based on a similar study of midbody microtubule depolymerization in fixed HeLa cells (43). Midbody formation was defined as the first appearance of an intercellular bridge containing a bulge and mostly condensed flanking microtubules, and abscission was defined as the first appearance of a gap lacking a detectable mCherry-tubulin signal in the midbody connecting the daughter cells. For live cell snapshots of EGFP-WDR5, EGFP-WDR5-S91K, and EGFP-WDR5-F133A, and EGFP-WDR5_71–173, HeLa cells were imaged 24 h after transient co-transfection with mCherry-tubulin and one of the above EGFP-containing plasmids using TurboFect (Thermo Scientific) at a 3:1 ratio of TurboFect to plasmid according to the manufacturer's instructions. To quantify the cytokinesis phenotype of cells overexpressing EGFP or EGFP-WDR5_71–173, live cell exposures were captured once every 30 min for a maximum of 3 h following mature midbody formation (defined by the presence of a midbody bulge and mostly condensed flanking midbody microtubules). Cell death was defined by extreme membrane blebbing events in one or both connected daughter cells that led to the collapse of overall cell shape.

Confocal Fluorescence Microscopy and Quantification of Midbody H3K4MT—Cells co-expressing WDR5-EGFP (pLVXpuro) and mCherry (pLNCX) or EGFP (pLVXpuro) and mCherry (pLNCX) were immunostained for acetylated tubulin as described above and imaged on an Olympus FLV1000S spectral laser scanning confocal. A PlanApo N 60XOSC objective (N.A. = 1.4) was used throughout, with excitation laser lines at 405, 488, 559, and 635 nm for DAPI, EGFP, mCherry, and Cy5-conjugated secondary antibody, respectively. Images were captured as z-series of 8–15 planes each (0.5-μm steps). Quantification of WDR5 or EGFP midbody enrichment was performed on the middle z-slice in each series using ImageJ (National Institutes of Health). A profile plot (intensity *versus* distance) was constructed for EGFP, mCherry, and acetylated tubulin channels along a 6-μm linear selection overlaid on the midbody-acetylated tubulin signal. The center of the midbody dark zone was defined as the location on this line with the lowest acetylated tubulin signal, and peak mCherry or EGFP values were taken as the maximum intensity value within 1.5 μm of this dark zone center. The ratio of peak mCherry or EGFP signal to the average signal of a 1-μm length of midbody flanking

region immediately outside the boundary of the dark zone center (1.5 μm to 2.5 μm from the minimum acetylated tubulin point) was calculated as the fold enrichment of mCherry or EGFP in the dark zone compared with the flanking region.

Immunofluorescence Quantification—The following phenotypes were quantified in fixed cells using conventional fluorescence microscopy as described above. Multinucleated cells were counted using DAPI (1 μg/ml) as a nuclear marker and the lipophilic dye $DiOC_6$ (1 μg/ml) to visualize cell membranes. Cells containing two or more similarly sized nuclei within one cytoplasm were classified as multinucleated. At least 1000 cells per condition were counted, and data are presented as the mean ± S.E. of at least three independent experiments. Midbody width was measured from images acquired under nonsaturating exposure conditions. Using acetylated tubulin to visualize midbody microtubules, midbody width was measured at the thickest point for 100 cells per condition with ImageJ (National Institutes of Health). Data are presented as the mean ± S.E. of four independent experiments. Secondary ingressions, defined by at least one dark gap lacking tubulin or acetylated tubulin signal accompanied by narrower microtubules, were quantified in 100 cells per condition. Data represent the mean ± S.E. of five independent experiments. For quantification of nocodazole-induced microtubule disassembly in live cells, images acquired under nonsaturating exposure conditions were background-subtracted using ImageJ (National Institutes of Health); the midbody was bound with a freehand selection, and the average pixel intensity within this region was measured. Values for 15- and 30-min time points were normalized to the average midbody pixel intensity at 0 min in the same cell. For each group, $n = 11–22$ cells.

Statistical Analysis—All statistical tests were performed using IBM SPSS Statistics 20 (IBM). Unless otherwise specified, statistical significance was assessed by univariate ANOVA with Tukey's HSD post hoc, and data are presented as mean ± S.E. error bars. Homogeneity of variance was assessed using Levene's test. For all analyses, $\alpha = 0.05$.

RESULTS

WDR5 Localizes to the Midbody Dark Zone—Although WDR5 is generally thought to function in the nucleus, the EGFP fusion of WDR5 produced a stronger fluorescent signal in the midbody central dark zone than the neighboring areas in both HeLa (Fig. 1*a*) and RPE1 (Fig. 1*b*) cells. Because the fixation and permeabilization of cells during immunostaining can lead to imaging artifacts, particularly the differential extraction of some soluble proteins from the cytoplasm (44), we also performed fluorescence imaging of live HeLa cells stably expressing mCherry-tubulin (to label the midbody) and either EGFP or WDR5-EGFP. Although midbody-localized WDR5-EGFP was apparent in nearly all telophase cells, EGFP alone was not concentrated at this location in live cells (Fig. 1*c*). To confirm that WDR5 is indeed enriched in the dark zone, we performed a quantitative confocal microscopic analysis of HeLa cells co-expressing WDR5-EGFP and mCherry (a soluble protein expected to distribute uniformly throughout the midbody). As shown in Fig. 1, *d–f*, WDR5-EGFP was concentrated ~2.5-fold in the dark zone relative to mCherry. Because extreme overexpression of WDR5-EGFP might lead to a spurious localization at the midbody, we compared the degree of dark zone WDR5-EGFP enrichment in cells from the same stable line that expressed either high or low levels of WDR5-EGFP. Midbody WDR5-EGFP enrichment was found to be independent of the WDR5-EGFP expression level (Fig. 1*f*). Finally, we compared the degree of nonspecific midbody enrichment exhibited by EGFP or mCherry alone. Although the signal of EGFP alone is slightly enhanced within the midbody in fixed cells, this difference was not statistically significant relative to mCherry (Fig. 1*f*). Central dark zone proteins are typically inaccessible to antibodies (32, 45), which may explain why the midbody localization of WDR5 has not been reported previously.

The following observations suggest that the midbody localization of WDR5-EGFP is not a consequence of its association with lagging chromosomes, which are occasionally observed at the midbodies of dividing cells. First, lagging chromosomes were found in fewer than 10% of telophase HeLa cells (a number consistent with a previous report (46)), whereas midbody-localized WDR5-EGFP was present in virtually all telophase cells. Second, the midbody EGFP signal of WDR5 was readily detected when DAPI-labeled lagging chromosomes were absent (Fig. 1, *a*, *b,* and *d*). These results indicate that WDR5 can be found at the midbody independent of lagging chromosomes, and we therefore examined several known midbody-localized proteins for interaction with WDR5.

WDR5 Associates with Known Midbody Dark Zone and Ring Proteins—We generated RPE1 and HeLa cells stably expressing WDR5-EGFP and tested the interaction between WDR5-EGFP and known midbody proteins using co-immunoprecipitation. In addition to ASH2L, RbBP5, mDPY-30, and histone H3 (Fig. 2*a*), WDR5-EGFP efficiently co-immunoprecipitated with several dark zone and midbody ring proteins (PRC1, MKLP1, CYK4, and CEP55) in both RPE1 (Fig. 2*b*) and HeLa cells (Fig. 2*c*). The WDR5 fusion also co-immunoprecipitated, although to a lesser extent, with proteins known to be targeted to the midbody ring by their interaction with MKLP1, CYK4, and CEP55, including ECT2, ALIX, TSG101, and CHMP1B. Consistent with the dark zone localization of WDR5-EGFP revealed by our imaging analysis, little or undetectable association between WDR5-EGFP and Aurora B kinase (Fig. 2, *b* and *c*), a protein flanking the dark zone, was observed. Interestingly, some dark zone (KIF4) or midbody ring (Centriolin) proteins also exhibited little or undetectable co-immunoprecipitation with WDR5-EGFP (Fig. 2, *b* and *c*), suggesting that WDR5 preferentially associates with a subset of dark zone/ring proteins. Compared with EGFP alone, we noticed that stable expression of WDR5-EGFP led to an increase in the levels of PRC1, MKLP1, CYK4, and CEP55 in RPE1 cells (Fig. 2*b*, *lysate lane*). Subsequent analysis using nontransfected RPE1 cells showed that this observation was due to a down-regulation of these proteins in EGFP-expressing RPE1 cells. However, co-immunoprecipitation of WDR5-EGFP with these proteins cannot be simply explained by the increased protein levels, because HeLa cells stably expressing EGFP or WDR5-EGFP have similar levels of PRC1, MKLP1, CYK4, and CEP55 (Fig. 2*c*, *lysate lane*). Because many of the midbody proteins found to associate with WDR5-EGFP interact directly or indirectly with microtubules,

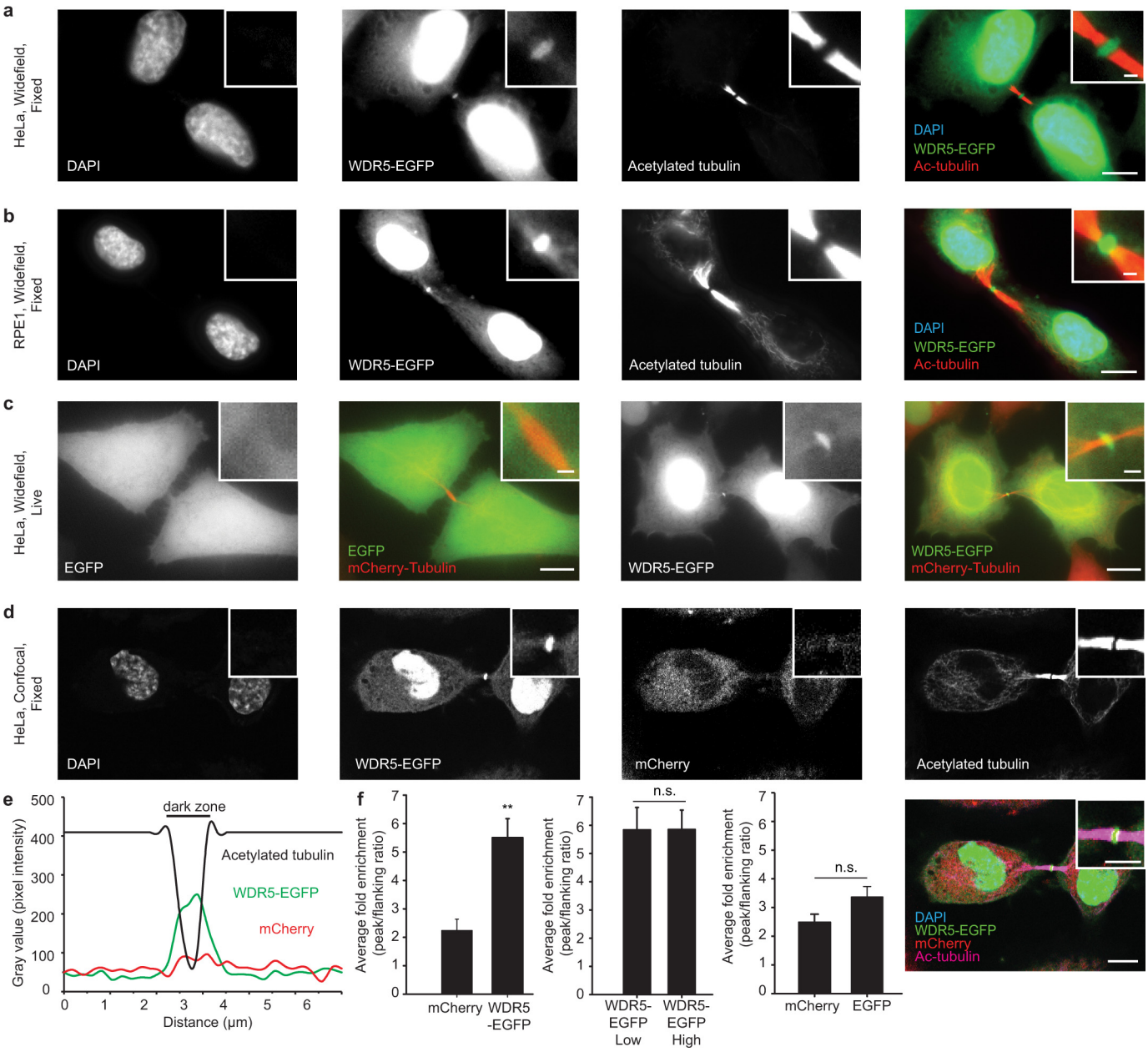

FIGURE 1. **WDR5-EGFP localizes to the midbody during cytokinesis.** *a* and *b,* in addition to the nuclear localization of WDR5-EGFP, widefield fluorescence microscopy of fixed HeLa (*a*) or RPE1 (*b*) cells stably expressing WDR5-EGFP revealed WDR5-EGFP enrichment at the central dark zone of the midbody (indicated by flanking acetylated tubulin staining). *c,* midbody enrichment of WDR5-EGFP (*right*) was verified in live HeLa cells, although EGFP alone did not localize to the midbody under these conditions (*left*). *Large scale bars,* 10 μm. *Inset scale bars,* 1 μm. *d,* midbody fluorescent signals of WDR5-EGFP, mCherry (a soluble cytoplasmic probe), and acetylated tubulin are depicted in one representative confocal section taken from the middle of a z-series of a HeLa cell stably expressing WDR5-EGFP and mCherry. *Large scale bar,* 10 μm. *Inset scale bar,* 5 μm. *e,* for the images in *d*, a line plot of pixel intensity *versus* distance measured from a 6-μm line selection over the midbody indicates ~2.5× greater enrichment of WDR5-EGFP fluorescence at the central dark zone compared with the signal from mCherry. The dark zone is indicated by a lack of acetylated tubulin staining. *f,* statistical analysis (for WDR5-EGFP, $n = 11$ cells; for EGFP, $n = 12$ cells) confirms that WDR5-EGFP displays greater concentration at the central dark zone compared with mCherry (*left*). This phenotype was independent of WDR5-EGFP expression level, because the degree of WDR5-EGFP enrichment within the midbody dark zone was nearly equivalent in cells expressing high ($n = 11$ cells) or low ($n = 10$ cells) levels of WDR5-EGFP (*center*). Although EGFP alone ($n = 12$ cells) also exhibits ~35% greater midbody enrichment than mCherry ($n = 12$ cells) in fixed cells, this difference was not statistically significant (*right*). Univariate ANOVA was used for all statistical analyses, ** indicates $p < 0.001$, *n.s.* indicates $p > 0.05$. Data represent means ± S.E.

we asked whether tubulin itself co-immunoprecipitates with WDR5-EGFP. Although nearly all β-tubulin remains soluble under our lysis and immunoprecipitation conditions, it does not appreciably associate with WDR5-EGFP (Fig. 2*d*). This result suggests that WDR5-EGFP associates with midbody proteins independent of a direct interaction with microtubules.

To address the issue of whether co-immunoprecipitation of midbody proteins with WDR5-EGFP reflects the behavior of endogenous WDR5 at the midbody, we first examined the degree of WDR5-EGFP overexpression in this HeLa stable line. As shown in Fig. 3*a*, WDR5-EGFP is moderately overexpressed (~5-fold greater abundance) compared with endogenous

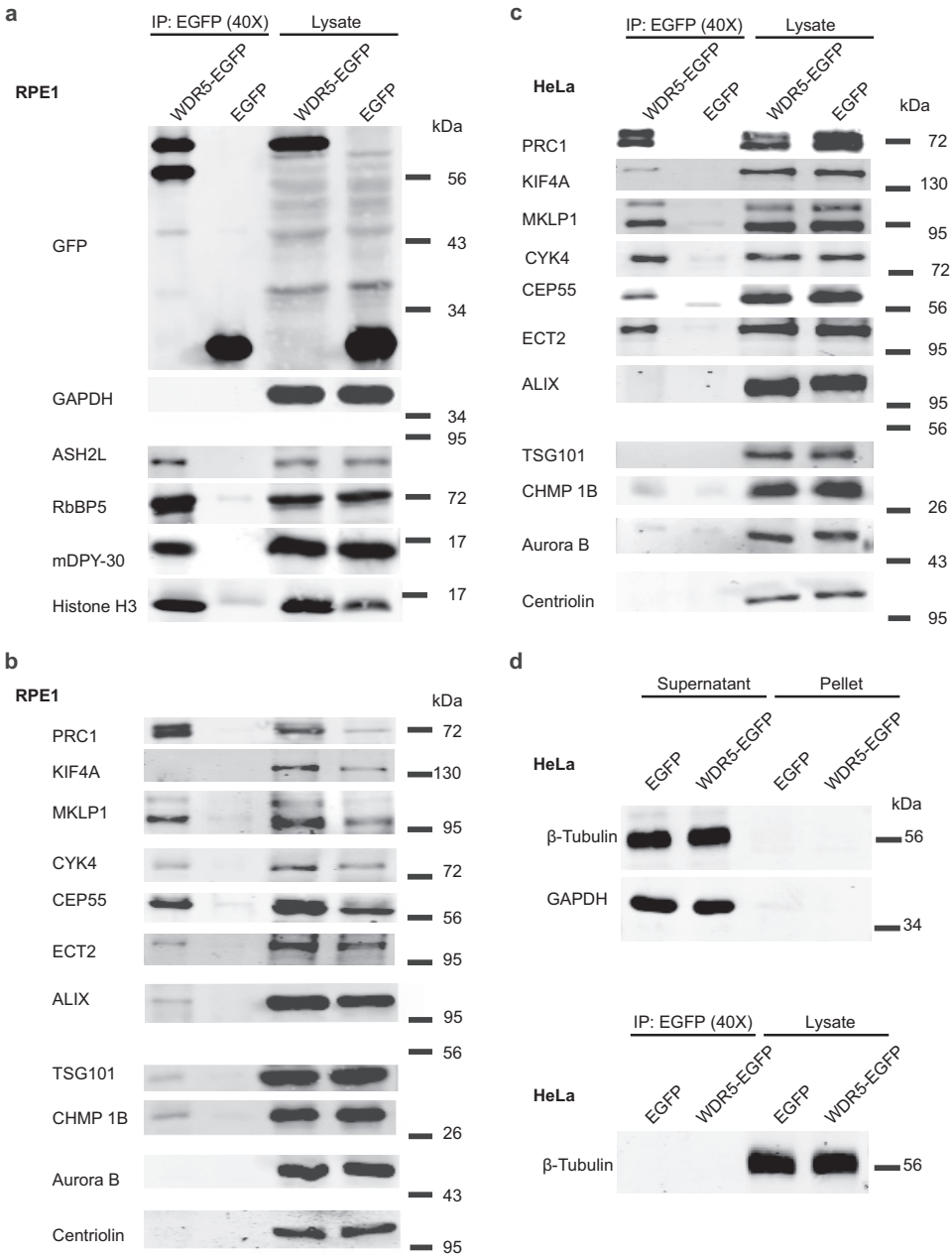

FIGURE 2. **WDR5-EGFP associates with a subset of midbody dark zone and ring proteins.** *a,* WDR5-EGFP co-immunoprecipitates with known histone H3 lysine 4 methyltransferase complex members ASH2L, RbBP5, mDPY-30, and histone H3 in RPE1 cells stably expressing WDR5-EGFP. *b* and *c,* additionally, PRC1 (a dark zone protein) as well as MKLP1, CYK4, and CEP55 (three midbody ring proteins) efficiently co-immunoprecipitate with WDR5-EGFP in both RPE1 (*b*) and HeLa (*c*) cells stably expressing WDR5-EGFP. ECT2, ALIX, TSG101, and CHMP1B (four proteins recruited to the midbody ring by MKLP1, CYK4, and CEP55) can also be detected in WDR5-EGFP immunoprecipitates at a lower level. In contrast, KIF4A (another dark zone protein), Centriolin (another ring protein), and Aurora B kinase (a flanking protein) are barely detectable in the same immunoprecipitates. *d,* although nearly all cellular β-tubulin was soluble under these lysis and immunoprecipitation conditions (*top*), β-tubulin did not co-immunoprecipitate with WDR5-EGFP (*bottom*). The lysate lanes contain 1/40 of the protein amounts used in immunoprecipitation. Approximate molecular masses are noted at the *right* of Western blots in kDa.

WDR5. Furthermore, we confirmed that endogenous WDR5 co-immunoprecipitates with MKLP1 and CYK4 from HeLa spindle/midbody isolate under the stringent conditions required to solubilize the isolated spindle/midbody pellet (1% Nonidet P-40, 0.5% sodium deoxycholate, and 0.1% SDS) (Fig. 3*b*), suggesting a specific interaction that is independent of WDR5 epitope tagging or exogenous expression. Moreover, a larger fraction of endogenous WDR5 is present in isolated midbodies compared with lamin A (a nuclear marker), Hsp70, or GAPDH (two proteins predominantly localized to the cytoplasm) (Fig. 3*c*). These results suggest that endogenous WDR5 is a *bona fide* component of the midbody.

Previously, large scale proteomic studies using multidimensional protein identification technology (MudPIT) mass spectrometry identified WDR5 as a component of the mitotic spindle (47) but not of the midbody (41) in CHO cells. Although MudPIT is especially useful for bulk proteomic analysis, its detection sensitivity for specific proteins can be limited by factors, including low abundance (48), small size (49), presence of

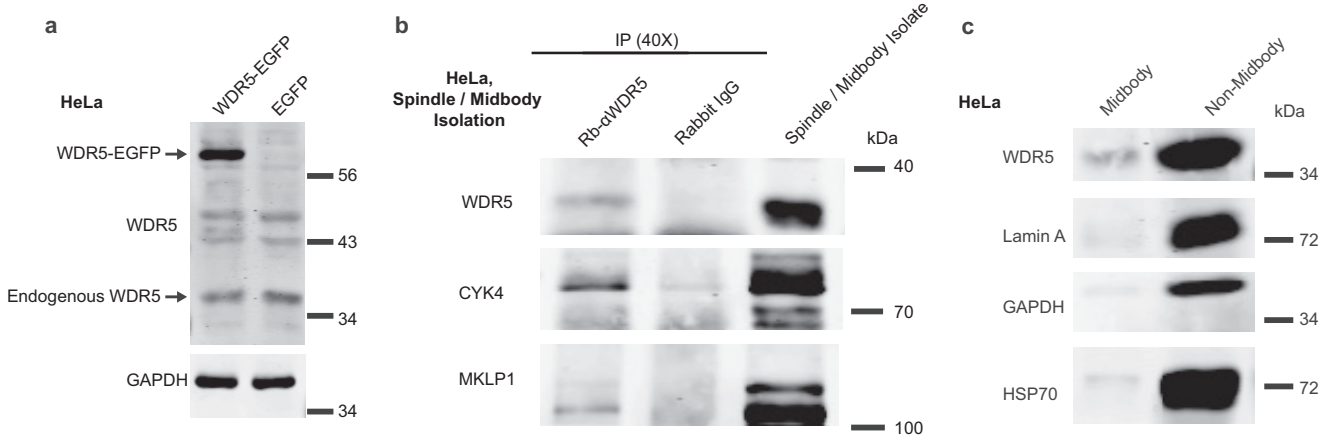

FIGURE 3. **Endogenous WDR5 is present in HeLa midbodies and associates with MKLP1-CYK4.** *a,* WDR5-EGFP is moderately overexpressed (~5-fold greater abundance relative to endogenous WDR5 as quantified by LI-COR Odyssey Infrared Imaging System) in the HeLa stable line used for co-immunoprecipitation experiments. *b,* endogenous WDR5 co-immunoprecipitates with both CYK4 and MKLP1 from HeLa spindle/midbody isolate under stringent immunoprecipitation conditions (1% Nonidet P-40, 0.5% sodium deoxycholate, and 0.1% SDS). The spindle/midbody isolate lane contains 1/40 of the protein amounts used in immunoprecipitation. *c,* larger fraction of endogenous WDR5 is present in isolated midbodies compared with lamin A (a nuclear marker), Hsp70, or GAPDH (two proteins predominantly localized to the cytoplasm). Because the non-midbody sample consists of equal parts supernatant and spindle (see "Experimental Procedures"), the non-midbody and midbody lanes were loaded at a 2:1 ratio so that extract from each of these three fractions is present in equal proportion with respect to cell number. For detection of GAPDH and HSP70, sample loading volumes were reduced by half to accommodate the higher non-midbody signal intensity. Approximate molecular masses are noted at the *right* of Western blots in kDa.

modifications (50), and amino acid composition (50). Some combination of these limitations may explain why MudPIT did not identify WDR5 in purified midbodies despite the presence of nuclear contamination (1 nucleus per 60 to 70 midbodies), and other nuclear proteins (41).

Knockdown of WDR5 Increases Multinucleation—The midbody localization of WDR5 raises the possibility that it might play a role in cytokinesis. Because multinucleation is a hallmark of cytokinesis failure (23, 27), we determined the fraction of cells containing two or more nuclei in HeLa cells stably expressing a nontargeting control shRNA or either of two different shRNAs targeting WDR5. Both WDR5 shRNAs increased the number of multinucleated cells relative to the control shRNA (Fig. 4, *a* and *b*). To obtain a more uniform knockdown efficiency, we generated clonal HeLa cell lines stably expressing WDR5 shRNA 1. Although WDR5 could not be depleted by more than 80% in any of the clones tested (Fig. 4*e*, ~55 to 72% knockdown), all clones exhibited significantly increased numbers of multinucleated cells compared with two clones derived from the control shRNA (Fig. 4, *c* and *d*). Because clones derived from four additional WDR5 shRNAs expressed even higher levels of residual WDR5 (data not shown), further experiments were performed using clones 6 and 8 derived from WDR5 shRNA 1, both of which exhibit an intermediate level of WDR5 knockdown and multinucleation (Fig. 4, *c* and *d*). Moreover, the multinucleation phenotype exhibited by clones 6 and 8 was mostly rescued by stable expression of HA-tagged mouse WDR5 (mWDR5-HAC), which encodes an identical amino acid sequence to human WDR5 but is resistant to shRNA 1 (Fig. 4*f*). It remains possible that epitope tagging or nonphysiological expression levels of mWDR5-HAC may hinder the full rescue of the multinucleation phenotype to control levels.

Knockdown of WDR5 Impairs Abscission but Not Furrow Ingression—To further examine the role of WDR5 in cytokinesis, we performed fluorescent live cell imaging of cytokinesis in clonal WDR5 knockdown HeLa stable lines. Although knockdown of WDR5 had little effect on the early events of cytokinesis, including cleavage furrow ingression and midbody maturation (see below), it significantly delayed abscission (Fig. 5*a*; only those cells that completed abscission were included). Pairwise comparisons revealed significantly longer mean abscission times in both WDR5 knockdown clonal lines compared with either control clone (ANOVA with Tukey's HSD post hoc, $p < 0.001$). Midbody abscission was defined as the sudden appearance of a gap in the mCherry-tubulin signal connecting the daughter cells (*arrows* in Fig. 5*b*). Appearance of this gap was not due to photobleaching of mCherry-tubulin based on the short duration of the exposures (<200 ms per exposure) as compared with the rate of mCherry-tubulin photobleaching in our system (Fig. 5*f*; ~1% signal loss/s of continuous exposure). Although ~8% multinucleation is observed in WDR5 knockdown clones 6 and 8, our live cell imaging data did not reveal any instances of furrow regression in control or WDR5 knockdown stable lines ($n = 13–21$ cells per group). It is worth noting that a recent study indicates that even if depletion of a protein yields 5–10% multinucleation, the rate of regression could be as low as ~1%, and it may be restricted to a minor subset of telophase cells, for example those containing lagging chromosomes (51).

Knockdown of WDR5 Delays the Formation of Secondary Ingressions—To gain insight into the mechanism by which WDR5 facilitates abscission, we asked whether WDR5 knockdown affects the formation of secondary ingressions, a process preceding the final scission and characterized by gaps or narrowing in the midbody microtubules adjacent to the dark zone. We investigated secondary ingression formation by measuring the time between the formation of mature midbodies and the appearance of secondary ingressions using the live cell imaging data set previously described in Fig. 5*a*. Our analysis shows that the formation of secondary ingressions is significantly delayed in WDR5 knockdown cells (Fig. 5*c*), yet the time between anaphase onset and midbody maturation is not substantially

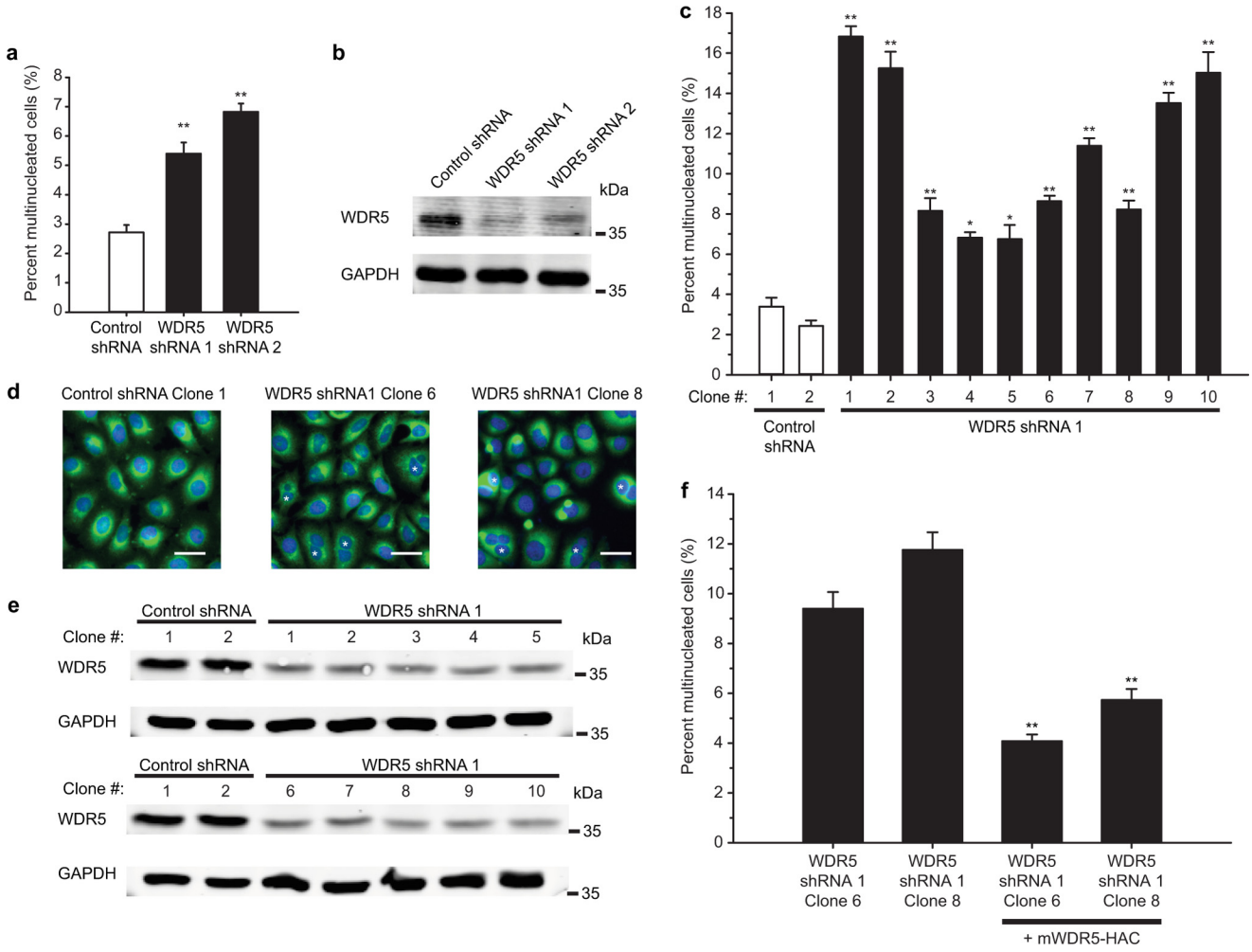

FIGURE 4. **Knockdown of WDR5 increases multinucleation.** *a,* stable knockdown of WDR5 in HeLa cells using either of two different shRNAs increases multinucleation ($n = 6–13$ independent experiments; ** indicates $p < 0.001$). *b,* efficacy of WDR5 knockdown by shRNAs 1 and 2 in pooled HeLa stable lines. *c,* knockdown of WDR5 in clonal HeLa stable lines increases multinucleation in all clones tested ($n = 4–8$ independent experiments; ** indicates $p < 0.001$; * indicates $p < 0.01$). *d,* multinucleated cells (labeled *) are present at a higher frequency in representative fields from two WDR5 shRNA 1 clonal lines compared with a clonal line expressing the control shRNA. *Scale bar,* 50 μm. Nuclei and cell membranes are visualized with DAPI and $DiOC_6$, respectively. *e,* quantitative Western blot analysis shows that WDR5 was moderately depleted (~55–72%) in clones stably expressing shRNA 1, although four other shRNAs targeting WDR5 had less effect (data not depicted). *f,* stable expression of HA-tagged mouse WDR5, which is resistant to shRNA 1, rescues the multinucleation phenotype in two WDR5 shRNA 1 clonal lines ($n = 6–7$ independent experiments, ** indicates $p < 0.001$). At least 1000 cells were counted per sample for each independent multinucleation experiment, and all statistical analyses were performed using ANOVA with Tukey's HSD post hoc. Data represent means ± S.E. Approximate molecular masses are noted at the *right* of Western blots in kDa.

affected (Fig. 5*d*). Although completion of final abscission after secondary ingression is also delayed in WDR5 knockdown cells (Fig. 5*g*, ANOVA with Tukey's HSD post hoc, $p < 0.05$), this duration represents only ~20% of the total delay observed in Fig. 5*a*. Consistent with this phenotype, WDR5 knockdown cells examined after fixation display a reduced fraction of telophase cells containing a secondary ingression (Fig. 5*e*, 15% for control clones *versus* 8%, and 7% for WDR5 knockdown clones 6 and 8, respectively). Taken together, our data suggest that WDR5 promotes abscission primarily by facilitating the formation of secondary ingressions.

Knockdown of WDR5 Leads to Increased Nocodazole Resistance of Midbody Microtubules—Secondary ingression formation depends on midbody microtubule disassembly and FIP3-positive recycling endosomes (37, 38). Compared with the telophase midbody microtubules of control cells, those of WDR5 knockdown HeLa cells occupy a larger area (Fig. 6*a*, ~30–35% greater width), raising the possibility that the disassembly of midbody microtubules may be impaired in these knockdown cells. To directly test whether this is the case, we added 10 μM nocodazole to control or WDR5 knockdown cells after midbody maturation and utilized live cell imaging to monitor microtubule disassembly within the midbody. Indeed, we found that the midbody microtubules of WDR5 knockdown cells are more resistant to nocodazole, compared with those of control cells (Fig. 6, *b* and *c*). These observations suggest that a defect in midbody microtubule disassembly may account for the delayed formation of secondary ingressions in WDR5 knockdown cells.

Mutations within the Central Arg-binding Cavity of WDR5 Impair Its Accumulation at the Midbody Dark Zone—Elucidation of the specific factor(s) that confers the midbody targeting of WDR5 may provide further insight into the function of midbody-localized WDR5. Although several studies have examined

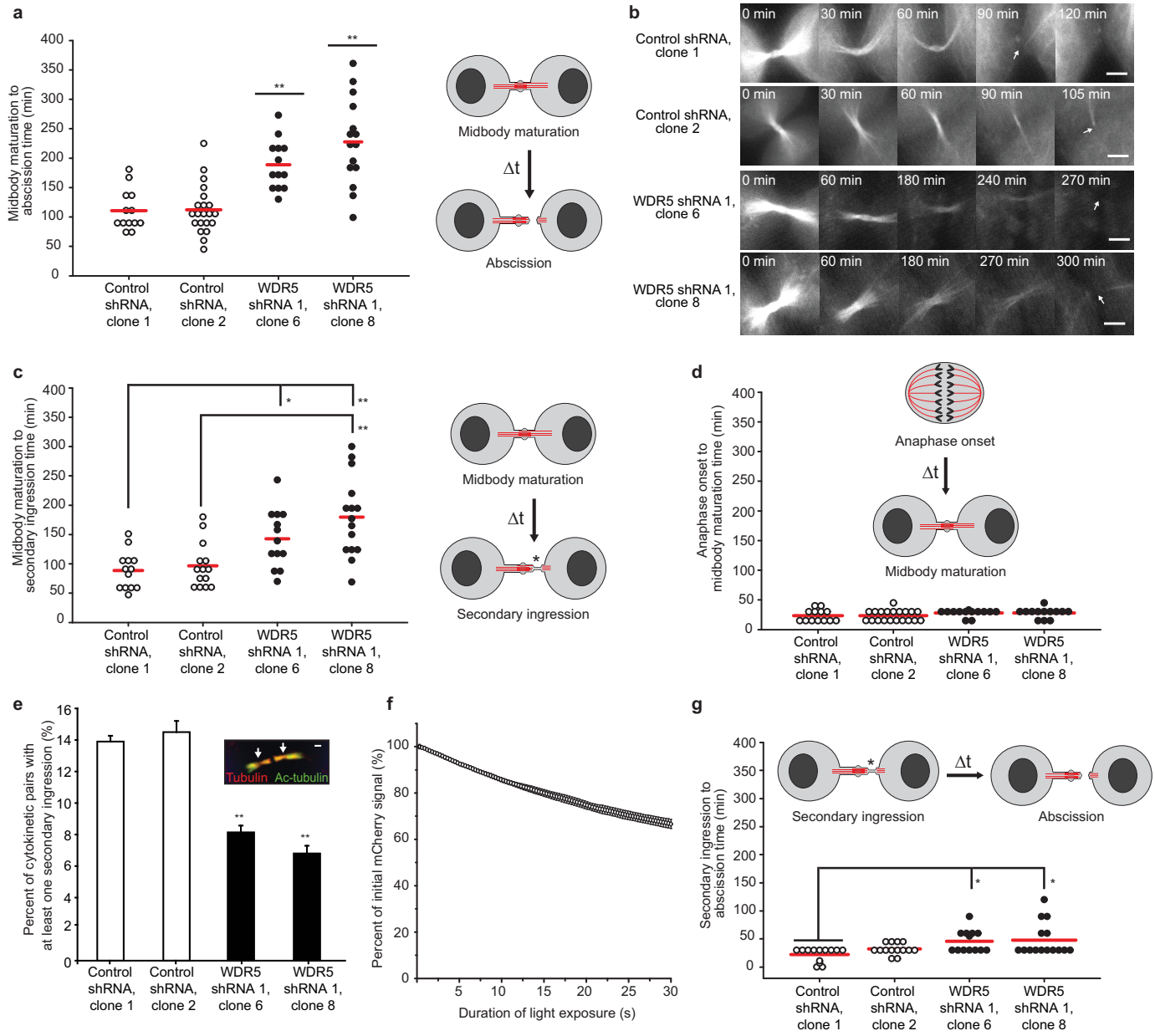

FIGURE 5. **Knockdown of WDR5 delays secondary ingression formation and abscission.** *a,* live cell imaging indicates that the duration between mature midbody formation and final abscission is significantly greater in WDR5 knockdown HeLa stable lines (ANOVA with Tukey's HSD post hoc; ** indicates $p < 0.001$ *versus* both control shRNA clones). Each point on the dot density plot represents a cell that completed abscission ($n = 13$–21 cells per group), and *red bars* indicate group means. *b,* representative time-lapse live imaging frame is shown for each cell line analyzed. Mature midbody formation (0 min) was characterized by the presence of mostly condensed flanking microtubules and a midbody bulge. Abscission was defined as the sudden appearance of a gap in mCherry-tubulin signal (*arrows*). *Scale bars,* 5 μm. *c,* analysis of the live cell imaging data collected in *b* shows that knockdown of WDR5 delays secondary ingression formation. Only cells with clearly visible secondary ingressions were included ($n = 13$–15 cells per group); * indicates $p < 0.05$; ** indicates $p < 0.001$ for ANOVA with Tukey's HSD post hoc. *d,* duration between anaphase onset and mature midbody formation is not significantly delayed in clonal WDR5 knockdown HeLa stable lines. *e,* number of cells exhibiting secondary ingressions decreased in clonal WDR5 knockdown HeLa stable lines as compared with control cells ($n = 5$ independent experiments of at least 100 cells per group, ANOVA with Tukey's HSD post hoc; ** indicates $p < 0.0001$). As shown in the representative image, the secondary ingression was detected by a lack of both acetylated tubulin and tubulin staining at a midbody site adjacent to the dark zone (*arrows*). Data represent means ± S.E. *Scale bar,* 1 μm. *f,* rate of mCherry-tubulin photobleaching was ~1% signal loss/s of continuous exposure ($n = 5$ HeLa cells exposed to 100 consecutive 300-ms exposures). This rate is too slow to explain the sudden (within ~1 s of acquisition time) disappearance of signal observed during ingression or abscission events. Data represent means ± S.D. *g,* knockdown of WDR5 slightly delayed the duration between secondary ingression and final abscission (ANOVA with Tukey's HSD post hoc; * indicates $p < 0.05$).

the sequence and structural features required for specific WDR5 protein-protein interactions (15, 19, 52), the mechanisms that regulate its subcellular localization remain largely unexplored. In principle, the top, bottom, and sides of the WDR5 β-propeller are all potential surfaces for protein-protein interactions (53), although interactions that involve a site located at the top (acidic end) of the WDR5 central cavity are best characterized (18, 19, 54). This cavity binds to an ARA*X* containing "WIN" (WDR5-interacting) motif in the target protein. To determine whether interactions at this site influence the midbody localization of WDR5, we investigated the localization of EGFP fusions of WDR5 containing either the S91K or

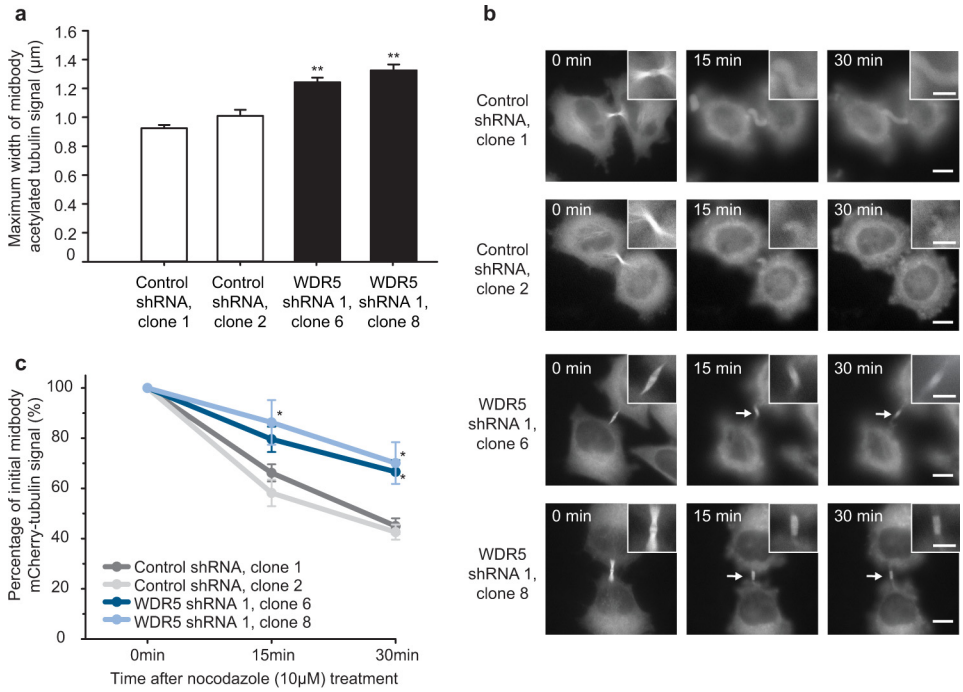

FIGURE 6. **Midbody microtubule disassembly by nocodazole is delayed in WDR5 knockdown cells.** *a,* knockdown of WDR5 in clonal HeLa stable lines increases the width of midbody acetylated tubulin signal. Midbody width was measured at the thickest flanking region ($n = 4$ independent experiments of at least 100 cells per group, ANOVA with Tukey's HSD post hoc; ** indicates $p < 0.0001$). Acetylated tubulin images for width quantification were acquired under nonsaturating conditions using a constant exposure time and light intensity. *b,* representative time-lapse live imaging frames of clonal HeLa stable lines co-expressing mCherry-tubulin and control or WDR5 shRNAs. A resistance of WDR5 knockdown cells to midbody microtubule disassembly is apparent after 15 and 30 min of incubation with 10 μM nocodazole compared with two control shRNA clones (nocodazole-resistant microtubule bundles are indicated by *arrows*). *Large scale bars,* 10 μm. *Inset scale bars,* 5 μm. *c,* quantitative analysis of the nocodazole resistance of midbody microtubules in clonal WDR5 knockdown HeLa stable lines. Data represent means ± S.E., $n = 11$–22 cells per group, and * indicates $p < 0.05$ by ANOVA with Tukey's HSD post hoc.

F133A point mutation, each of which blocks the binding of WIN motif-containing proteins to WDR5 (11, 18, 19), in HeLa cells. Interestingly, although wild type EGFP-WDR5 localizes to the nucleus and midbody (Fig. 7*a*), mutation of either S91K or F133A substantially reduced the midbody localization of WDR5 without affecting its nuclear localization in all cells examined (Fig. 7, *b* and *c*). This result suggests that distinct mechanisms control the midbody and nuclear targeting of WDR5 and indicates that a WIN motif-containing protein likely recruits WDR5 to the midbody dark zone.

WDR5 Contains a Midbody Targeting Domain and Its Overexpression Leads to Delayed Abscission or Cell Death during Cytokinesis—Based on the observation that mutations within the arginine binding cavity of WDR5 greatly reduce its midbody (but not nuclear) localization, it is possible that uncharacterized structural features of WDR5 in the vicinity of this pocket facilitate its selective targeting to the midbody. Indeed, an EGFP fusion of a 103-amino acid truncation of WDR5 (positions 71–173), which contains many of the residues required for efficient binding to WIN motifs in histone H3 and MLL1 (18, 19, 55–57), exhibited a highly enriched EGFP signal at the midbody with relatively little EGFP accumulation in the nucleus (Fig. 7*d*). The selective enrichment of EGFP-WDR5(71–173) at the midbody prompted us to examine whether cells transiently expressing this construct displayed a disrupted cytokinesis phenotype. Although most cells overexpressing EGFP alone completed cytokinesis normally, overexpression of EGFP-WDR5(71–173) led to either cell death during cytokinesis or abscission delays greater than 3 h in 90% of the cells imaged (Fig. 7*e*), presumably due to the dominant-negative effect of this truncation. These observations indicate that WDR5 contains a domain sufficient for its midbody (but not nuclear) targeting and suggest that midbody-localized WDR5 functions in the completion of cytokinesis.

DISCUSSION

Because of the intimate link between H3K4 methylation and transcription (58), the H3K4MT literature almost exclusively focuses on the roles of these complexes in the nucleus, and much less is known regarding the cytoplasmic localization and function of H3K4MT subunits. This study identifies a novel function of WDR5 in abscission. We show that the EGFP fusion of WDR5 localizes within the mature midbody during cytokinesis (Figs. 1–3) in the absence of DNA. Knockdown of WDR5 increases the prevalence of multinucleated cells (Fig. 4), a hallmark of cytokinesis failure. Importantly, depletion of WDR5 prolongs the duration between midbody maturation and final scission without significantly affecting the time between anaphase and midbody maturation (Fig. 5). Collectively, these data show that WDR5 promotes abscission, possibly by performing a local function at the midbody. In this regard, it is interesting that that the S91K and F133A mutations impair the localization of WDR5 to the midbody (but not to the nucleus), and that WDR5(71–173) is selectively targeted to the midbody and induces cytokinesis failure (Fig. 7, *d* and *e*). These observations suggest that identification of the putative WIN motif-containing midbody protein may allow future dissection of nuclear and midbody functions of WDR5. In addition to multinucleation

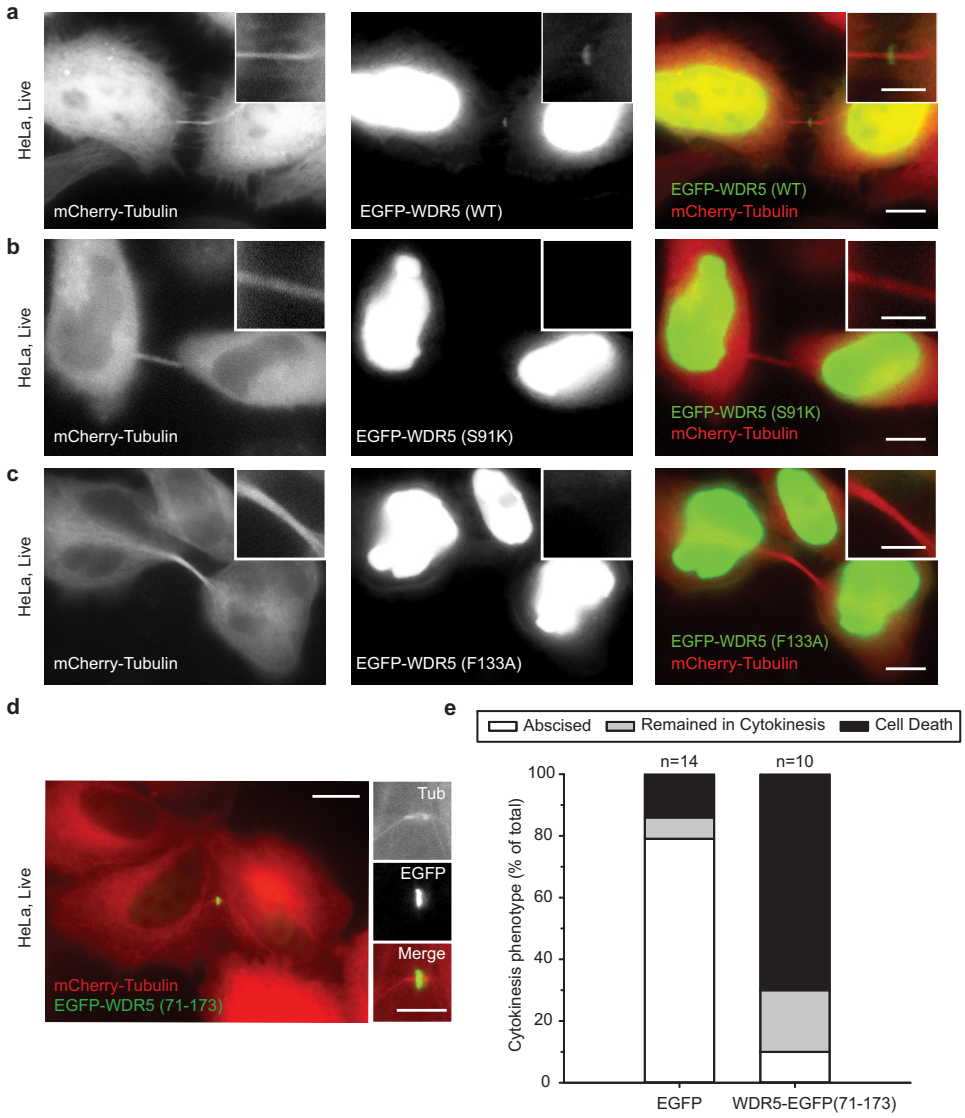

FIGURE 7. **Structural features of WDR5 that facilitate its localization to the midbody.** *a,* live cell imaging confirmed the presence of wild type EGFP-WDR5 at the midbody. *b* and *c,* in contrast, the point mutations S91K (*b*) or F133A (*c*), which are known to block the binding of WDR5 to arginine motif-containing proteins *in vitro* (for example, histone H3, MLL1), substantially reduce the accumulation of EGFP-WDR5 at the midbody dark zone. *d,* EGFP fused to a 103-amino acid truncation of WDR5 (positions 71–173) efficiently localizes to the midbody dark zone with greatly reduced accumulation in the nucleus in live HeLa cells. *e,* transient overexpression of EGFP-WDR5(71–173) frequently led to cell death during cytokinesis or abscission delays of >3 h, although ~80% of cells overexpressing EGFP alone completed cytokinesis normally. *Large scale bars,* 10 μm. *Inset scale bars,* 5 μm.

and abscission delay, cell death during cytokinesis is also associated with the perturbation of several different cytokinesis regulators, either via knockdown (37, 59 – 62) or by ectopic expression of the midbody-targeting region of the protein (59). However, the mechanism of cytokinesis-associated cell death has not been extensively investigated.

To the best of our knowledge, WDR5 is the first H3K4MT subunit to be found at the midbody, which raises several intriguing questions regarding the mechanism and functional significance of its recruitment to this location Recently, transient knockdown of WDR5 and other H3K4MT complex members, including RbBP5, ASH2L, mDPY-30, and the catalytic subunit. MLL1, was reported to increase the degree of multinucleation in U2OS cells, although the underlying mechanism was not explored (63). Given this finding, one possibility is that some combination of additional H3K4MT subunits localizes to the midbody and functions together with WDR5 in the context of a methyltransferase complex or subcomplex. In this regard, histone H3 phosphorylated at either Ser-10 or Thr-11 was also previously reported to reside at the midbody in MCF-7 and CHO cells (64, 65). Given the difficulty of obtaining highly specific immunostaining of midbody proteins, this result should be verified with EGFP-histone H3 in live cells. It is also possible that an H3K4MT methyltransferase complex or subcomplex promotes abscission by methylating novel non-histone midbody substrate(s). The recent observation that a midbody-localized demethylase ALKBH4 facilitates cytokinesis by demethylating actin at the cleavage furrow suggests that regulated methylation/demethylation of non-histone proteins may be important for proper cytokinesis (66).

Alternatively, WDR5 may assemble with a set of non-H3K4MT midbody effectors to perform an activity besides pro-

tein methylation. Although our immunoprecipitation data suggest that EGFP-WDR5 robustly associates with at least five different midbody proteins (Fig. 2, *b* and *c*; *PRC1, CYK4, MKLP1, CEP55,* and *ECT2*), it seems unlikely that all are direct interacting partners. If WDR5 performs a scaffolding role for non-H3K4MT proteins, as is common for other WD40 β-propellers (53), it will be important to identify the direct midbody binding partner(s). In this aspect, our study suggests that a WIN motif-containing protein directly binds to the central Arg-binding cavity of WDR5 and targets it to the midbody. The WIN domain has been defined and structurally characterized using 12–19 amino acid peptides designed around six central residues that are highly conserved among human MLL-SET family catalytic subunits in the pattern G(S/C/A)AR(A/S)E (54, 67, 68). However, a 3-mer peptide containing the central invariant alanine and arginine residues (acetyl-ARA-NH_2) was recently shown to have a nearly identical K_i (0.12 μM) as the full 12-residue WIN peptide (0.16 μM) (69, 70), suggesting that the ARA peptide captures most of the high affinity interactions between the 12-mer WIN domain and WDR5. Similarly, an alanine-arginine motif is required for the high affinity interaction of WDR5 with the N terminus of histone H3 (ARTKQ) (71), suggesting that a minimal AR(AST) sequence within a putative midbody targeting protein may be sufficient to recruit WRD5.

Only two non-H3K4MT-binding interactions with WDR5 at this site have been characterized so far. WDR5 is required for efficient assembly of the nonspecific lethal complex in the nucleus, and the KANSL1 subunit of this complex binds to the central cavity of WDR5 via a WIN motif (72). Additionally, the influenza virus protein NS1, which primarily localizes to the nucleus of infected cells (73) and is thought to function as a histone mimic, contains two adjacent WIN motifs near its C terminus that bind WDR5 in a similar manner (74). Notably, none of these proteins have been reported to localize to the midbody or function in cytokinesis, suggesting that if WDR5 is recruited to the midbody by a protein other than SET/MLL or histone H3, its identity remains to be discovered. Of the midbody proteins that robustly co-immunoprecipitate with WDR5-EGFP (PRC1, MKLP1, CYK4, ECT2, and CEP55), only MKLP1 and ECT2 contain AR(AST) motifs (MKSARAK and QMDARAG, respectively), and whether either directly recruits WDR5 to the midbody remains to be determined.

Several observations indicate that WDR5 modulates the stability of midbody microtubules during abscission. First, the midbody microtubules in WDR5 knockdown cells are more resistant to nocodazole-mediated depolymerization (Fig. 6, *b* and *c*). Second, depletion of WDR5 results in a larger area of midbody microtubules compared with the control (Fig. 6*a*), and secondary ingression formation is delayed in these cells (Fig. 5, *c* and *e*). Both findings are consistent with a defect in midbody microtubule disassembly. Interestingly, PRC1 and MKLP1-CYK4, three known midbody-localized microtubule regulators, represent the most prominent proteins co-immunoprecipitated with WDR5 (Fig. 2, *b* and *c*). Identification of the direct binding partner(s) of WDR5 at the midbody should help elucidate the molecular mechanism by which WDR5 knockdown modulates microtubule disassembly. Another question that remains to be answered is the site where WDR5 exerts its effect on microtubules. Although WDR5-EGFP is highly enriched at the center of the midbody, it can also be detected at the midbody ring and along the flanking regions.[4]

In summary, we have uncovered an unexpected role of the H3K4MT regulatory subunit WDR5 in cytokinesis at the midbody. Considering the intimate relationship between cytokinesis and tumorigenesis, it will be important to elucidate the molecular mechanism by which WDR5 promotes abscission. Moreover, in addition to its tight association with human cancers (75), mutations or misregulation of H3K4MT subunits are directly linked to life span/aging (76), immunity (77), diabetes (78), mental retardation (79), and stem cell differentiation (80–82). Discovering nontranscriptional functions of H3K4MT subunits, as described here, is essential for understanding the association between these proteins and the above pathophysiological events.

Acknowledgments—We are grateful to M. Cosgrove for the WDR5 S91K and F133A constructs, W. I. Sundquist for the CHMP1B antibody, L. Johnson for the hTERT-RPE-1 cell line, and to the many undergraduates whose technical assistance contributed to this work. We also thank M. Glotzer for helpful suggestions, C. A. Vandenberg and K. R. Foltz for critically reading this manuscript, T. E. Kippin and K. K. Szumlinski for statistical advice, and Jennifer Knappe for editing assistance. We acknowledge the use of the NRI-MCDB Microscopy Facility and the Spectral Laser Scanning Confocal supported by the Office of The Director, National Institutes of Health Award S10OD010610.

REFERENCES

1. Martin, C., and Zhang, Y. (2005) The diverse functions of histone lysine methylation. *Nat. Rev. Mol. Cell Biol.* **6,** 838–849
2. Ng, S. S., Yue, W. W., Oppermann, U., and Klose, R. J. (2009) Dynamic protein methylation in chromatin biology. *Cell. Mol. Life Sci.* **66,** 407–422
3. Bernstein, B. E., Kamal, M., Lindblad-Toh, K., Bekiranov, S., Bailey, D. K., Huebert, D. J., McMahon, S., Karlsson, E. K., Kulbokas, E. J., 3rd, Gingeras, T. R., Schreiber, S. L., and Lander, E. S. (2005) Genomic maps and comparative analysis of histone modifications in human and mouse. *Cell* **120,** 169–181
4. Santos-Rosa, H., Schneider, R., Bannister, A. J., Sherriff, J., Bernstein, B. E., Emre, N. C., Schreiber, S. L., Mellor, J., and Kouzarides, T. (2002) Active genes are tri-methylated at K4 of histone H3. *Nature* **419,** 407–411
5. Ng, H. H., Robert, F., Young, R. A., and Struhl, K. (2003) Targeted recruitment of Set1 histone methylase by elongating Pol II provides a localized mark and memory of recent transcriptional activity. *Mol. Cell* **11,** 709–719
6. Guenther, M. G., Levine, S. S., Boyer, L. A., Jaenisch, R., and Young, R. A. (2007) A chromatin landmark and transcription initiation at most promoters in human cells. *Cell* **130,** 77–88
7. Shilatifard, A. (2008) Molecular implementation and physiological roles for histone H3 lysine 4 (H3K4) methylation. *Curr. Opin. Cell Biol.* **20,** 341–348
8. Hughes, C. M., Rozenblatt-Rosen, O., Milne, T. A., Copeland, T. D., Levine, S. S., Lee, J. C., Hayes, D. N., Shanmugam, K. S., Bhattacharjee, A., Biondi, C. A., Kay, G. F., Hayward, N. K., Hess, J. L., and Meyerson, M. (2004) Menin associates with a trithorax family histone methyltransferase complex and with the hoxc8 locus. *Mol. Cell* **13,** 587–597
9. Shilatifard, A. (2012) The COMPASS family of histone H3K4 methylases: mechanisms of regulation in development and disease pathogenesis. *Annu. Rev. Biochem.* **81,** 65–95

[4] D. Ma and J. Bailey, unpublished data.

10. Steward, M. M., Lee, J. S., O'Donovan, A., Wyatt, M., Bernstein, B. E., and Shilatifard, A. (2006) Molecular regulation of H3K4 trimethylation by ASH2L, a shared subunit of MLL complexes. *Nat. Struct. Mol. Biol.* **13,** 852–854
11. Dou, Y., Milne, T. A., Ruthenburg, A. J., Lee, S., Lee, J. W., Verdine, G. L., Allis, C. D., and Roeder, R. G. (2006) Regulation of MLL1 H3K4 methyltransferase activity by its core components. *Nat. Struct. Mol. Biol.* **13,** 713–719
12. Morgan, M. A., and Shilatifard, A. (2013) *Drosophila* SETs its sights on cancer: Trr/MLL3/4 COMPASS-like complexes in development and disease. *Mol. Cell. Biol.* **33,** 1698–1701
13. Ng, S. B., Bigham, A. W., Buckingham, K. J., Hannibal, M. C., McMillin, M. J., Gildersleeve, H. I., Beck, A. E., Tabor, H. K., Cooper, G. M., Mefford, H. C., Lee, C., Turner, E. H., Smith, J. D., Rieder, M. J., Yoshiura, K., *et al.* (2010) Exome sequencing identifies MLL2 mutations as a cause of Kabuki syndrome. *Nat. Genet.* **42,** 790–793
14. Southall, S. M., Wong, P.-S., Odho, Z., Roe, S. M., and Wilson, J. R. (2009) Structural basis for the requirement of additional factors for MLL1 SET domain activity and recognition of epigenetic marks. *Mol. Cell* **33,** 181–191
15. Odho, Z., Southall, S. M., and Wilson, J. R. (2010) Characterization of a novel WDR5-binding site that recruits RbBP5 through a conserved motif to enhance methylation of histone H3 lysine 4 by mixed lineage leukemia protein-1. *J. Biol. Chem.* **285,** 32967–32976
16. Shinsky, S. A., Hu, M., Vought, V. E., Ng, S. B., Bamshad, M. J., Shendure, J., and Cosgrove, M. S. (2014) A non-active-site SET domain surface crucial for the interaction of MLL1 and the RbBP5/Ash2L heterodimer within MLL family core complexes. *J. Mol. Biol.* **426,** 2283–2299
17. Schuetz, A., Allali-Hassani, A., Martín, F., Loppnau, P., Vedadi, M., Bochkarev, A., Plotnikov, A. N., Arrowsmith, C. H., and Min, J. (2006) Structural basis for molecular recognition and presentation of histone H3 by WDR5. *EMBO J.* **25,** 4245–4252
18. Ruthenburg, A. J., Wang, W., Graybosch, D. M., Li, H., Allis, C. D., Patel, D. J., and Verdine, G. L. (2006) Histone H3 recognition and presentation by the WDR5 module of the MLL1 complex. *Nat. Struct. Mol. Biol.* **13,** 704–712
19. Patel, A., Vought, V. E., Dharmarajan, V., and Cosgrove, M. S. (2008) A conserved arginine-containing motif crucial for the assembly and enzymatic activity of the mixed lineage leukemia protein-1 core complex. *J. Biol. Chem.* **283,** 32162–32175
20. Wang, Y. Y., Liu, L. J., Zhong, B., Liu, T. T., Li, Y., Yang, Y., Ran, Y., Li, S., Tien, P., and Shu, H. B. (2010) WDR5 is essential for assembly of the VISA-associated signaling complex and virus-triggered IRF3 and NF-κB activation. *Proc. Natl. Acad. Sci. U.S.A.* **107,** 815–820
21. van Nuland, R., Smits, A. H., Pallaki, P., Jansen, P. W., Vermeulen, M., and Timmers, H. T. (2013) Quantitative dissection and stoichiometry determination of the human SET1/MLL histone methyltransferase complexes. *Mol. Cell. Biol.* **33,** 2067–2077
22. Xu, Z., Gong, Q., Xia, B., Groves, B., Zimmermann, M., Mugler, C., Mu, D., Matsumoto, B., Seaman, M., and Ma, D. (2009) A role of histone H3 lysine 4 methyltransferase components in endosomal trafficking. *J. Cell Biol.* **186,** 343–353
23. Steigemann, P., Wurzenberger, C., Schmitz, M. H., Held, M., Guizetti, J., Maar, S., and Gerlich, D. W. (2009) Aurora B-mediated abscission checkpoint protects against tetraploidization. *Cell* **136,** 473–484
24. Fededa, J. P., and Gerlich, D. W. (2012) Molecular control of animal cell cytokinesis. *Nat. Cell Biol.* **14,** 440–447
25. Schiel, J. A., and Prekeris, R. (2013) Membrane dynamics during cytokinesis. *Curr. Opin. Cell Biol.* **25,** 92–98
26. Green, R. A., Paluch, E., and Oegema, K. (2012) Cytokinesis in animal cells. *Annu. Rev. Cell Dev. Biol.* **28,** 29–58
27. Fujiwara, T., Bandi, M., Nitta, M., Ivanova, E. V., Bronson, R. T., and Pellman, D. (2005) Cytokinesis failure generating tetraploids promotes tumorigenesis in p53-null cells. *Nature* **437,** 1043–1047
28. Lacroix, B., and Maddox, A. S. (2012) Cytokinesis, ploidy and aneuploidy. *J. Pathol.* **226,** 338–351
29. Steigemann, P., and Gerlich, D. W. (2009) Cytokinetic abscission: cellular dynamics at the midbody. *Trends Cell Biol.* **19,** 606–616
30. White, E. A., and Glotzer, M. (2012) Central spindlin: at the heart of cytokinesis. *Cytoskeleton* **69,** 882–892
31. Lee, K. Y., Davies, T., and Mishima, M. (2012) Cytokinesis microtubule organisers at a glance. *J. Cell Sci.* **125,** 3495–3500
32. Hu, C. K., Coughlin, M., and Mitchison, T. J. (2012) Midbody assembly and its regulation during cytokinesis. *Mol. Biol. Cell* **23,** 1024–1034
33. Guizetti, J., Schermelleh, L., Mäntler, J., Maar, S., Poser, I., Leonhardt, H., Müller-Reichert, T., and Gerlich, D. W. (2011) Cortical constriction during abscission involves helices of ESCRT-III-dependent filaments. *Science* **331,** 1616–1620
34. Elia, N., Sougrat, R., Spurlin, T. A., Hurley, J. H., and Lippincott-Schwartz, J. (2011) Dynamics of endosomal sorting complex required for transport (ESCRT) machinery during cytokinesis and its role in abscission. *Proc. Natl. Acad. Sci. U.S.A.* **108,** 4846–4851
35. Connell, J. W., Lindon, C., Luzio, J. P., and Reid, E. (2009) Spastin couples microtubule severing to membrane traffic in completion of cytokinesis and secretion. *Traffic* **10,** 42–56
36. Yang, D., Rismanchi, N., Renvoisé, B., Lippincott-Schwartz, J., Blackstone, C., and Hurley, J. H. (2008) Structural basis for midbody targeting of spastin by the ESCRT-III protein CHMP1B. *Nat. Struct. Mol. Biol.* **15,** 1278–1286
37. Schiel, J. A., Simon, G. C., Zaharris, C., Weisz, J., Castle, D., Wu, C. C., and Prekeris, R. (2012) FIP3-endosome-dependent formation of the secondary ingression mediates ESCRT-III recruitment during cytokinesis. *Nat. Cell Biol.* **14,** 1068–1078
38. Schiel, J. A., Park, K., Morphew, M. K., Reid, E., Hoenger, A., and Prekeris, R. (2011) Endocytic membrane fusion and buckling-induced microtubule severing mediate cell abscission. *J. Cell Sci.* **124,** 1411–1424
39. Morita, E., Colf, L. A., Karren, M. A., Sandrin, V., Rodesch, C. K., and Sundquist, W. I. (2010) Human ESCRT-III and VPS4 proteins are required for centrosome and spindle maintenance. *Proc. Natl. Acad. Sci. U.S.A.* **107,** 12889–12894
40. Xu, Z., Xia, B., Gong, Q., Bailey, J., Groves, B., Radeke, M., Wood, S. A., Szumlinski, K. K., and Ma, D. (2010) Identification of a deubiquitinating enzyme as a novel AGS3-interacting protein. *PLoS One* **5,** e9725
41. Skop, A. R., Liu, H., Yates, J., 3rd, Meyer, B. J., and Heald, R. (2004) Dissection of the mammalian midbody proteome reveals conserved cytokinesis mechanisms. *Science* **305,** 61–66
42. Lafaurie-Janvore, J., Maiuri, P., Wang, I., Pinot, M., Manneville, J. B., Betz, T., Balland, M., and Piel, M. (2013) ESCRT-III assembly and cytokinetic abscission are induced by tension release in the intercellular bridge. *Science* **339,** 1625–1629
43. Florindo, C., Perdigão, J., Fesquet, D., Schiebel, E., Pines, J., and Tavares, A. A. (2012) Human Mob1 proteins are required for cytokinesis by controlling microtubule stability. *J. Cell Sci.* **125,** 3085–3090
44. Schnell, U., Dijk, F., Sjollema, K. A., and Giepmans, B. N. (2012) Immunolabeling artifacts and the need for live-cell imaging. *Nat. Methods* **9,** 152–158
45. Euteneuer, U., and McIntosh, J. R. (1980) Polarity of midbody and phragmoplast microtubules. *J. Cell Biol.* **87,** 509–515
46. Rinaldo, C., Moncada, A., Gradi, A., Ciuffini, L., D'Eliseo, D., Siepi, F., Prodosmo, A., Giorgi, A., Pierantoni, G. M., Trapasso, F., Guarguaglini, G., Bartolazzi, A., Cundari, E., Schininà, M. E., Fusco, A., and Soddu, S. (2012) HIPK2 controls cytokinesis and prevents tetraploidization by phosphorylating histone H2B at the midbody. *Mol. Cell* **47,** 87–98
47. Bonner, M. K., Poole, D. S., Xu, T., Sarkeshik, A., Yates, J. R., 3rd, and Skop, A. R. (2011) Mitotic spindle proteomics in Chinese hamster ovary cells. *PLoS One* **6,** e20489
48. Liu, H., Sadygov, R. G., and Yates, J. R., 3rd. (2004) A model for random sampling and estimation of relative protein abundance in shotgun proteomics. *Anal. Chem.* **76,** 4193–4201
49. Washburn, M. P., Wolters, D., and Yates, J. R., 3rd (2001) Large-scale analysis of the yeast proteome by multidimensional protein identification technology. *Nat. Biotechnol.* **19,** 242–247
50. Swaney, D. L., McAlister, G. C., and Coon, J. J. (2008) Decision tree-driven tandem mass spectrometry for shotgun proteomics. *Nat. Methods* **5,** 959–964

51. Thoresen, S. B., Campsteijn, C., Vietri, M., Schink, K. O., Liestøl, K., Andersen, J. S., Raiborg, C., and Stenmark, H. (2014) ANCHR mediates Aurora-B-dependent abscission checkpoint control through retention of VPS4. *Nat. Cell Biol.* **16,** 550–560
52. Cao, F., Chen, Y., Cierpicki, T., Liu, Y., Basrur, V., Lei, M., and Dou, Y. (2010) An Ash2L/RbBP5 heterodimer stimulates the MLL1 methyltransferase activity through coordinated substrate interactions with the MLL1 SET domain. *PLoS One* **5,** e14102
53. Stirnimann, C. U., Petsalaki, E., Russell, R. B., and Müller, C. W. (2010) WD40 proteins propel cellular networks. *Trends Biochem. Sci.* **35,** 565–574
54. Zhang, P., Lee, H., Brunzelle, J. S., and Couture, J.-F. (2012) The plasticity of WDR5 peptide-binding cleft enables the binding of the SET1 family of histone methyltransferases. *Nucleic Acids Res.* **40,** 4237–4246
55. Han, Z., Guo, L., Wang, H., Shen, Y., Deng, X. W., and Chai, J. (2006) Structural basis for the specific recognition of methylated histone H3 lysine 4 by the WD-40 protein WDR5. *Mol. Cell* **22,** 137–144
56. Couture, J. F., Collazo, E., and Trievel, R. C. (2006) Molecular recognition of histone H3 by the WD40 protein WDR5. *Nat. Struct. Mol. Biol.* **13,** 698–703
57. Song, J.-J., and Kingston, R. E. (2008) WDR5 interacts with mixed lineage leukemia (MLL) protein via the histone H3-binding pocket. *J. Biol. Chem.* **283,** 35258–35264
58. Ruthenburg, A. J., Allis, C. D., and Wysocka, J. (2007) Methylation of lysine 4 on histone H3: intricacy of writing and reading a single epigenetic mark. *Mol. Cell* **25,** 15–30
59. Pohl, C., and Jentsch, S. (2008) Final stages of cytokinesis and midbody ring formation are controlled by BRUCE. *Cell* **132,** 832–845
60. Estey, M. P., Di Ciano-Oliveira, C., Froese, C. D., Bejide, M. T., and Trimble, W. S. (2010) Distinct roles of septins in cytokinesis: SEPT9 mediates midbody abscission. *J. Cell Biol.* **191,** 741–749
61. Tomas, A., Futter, C., and Moss, S. E. (2004) Annexin 11 is required for midbody formation and completion of the terminal phase of cytokinesis. *J. Cell Biol.* **165,** 813–822
62. Martz, M. K., Grabocka, E., Beeharry, N., Yen, T. J., and Wedegaertner, P. B. (2013) Leukemia-associated RhoGEF (LARG) is a novel RhoGEF in cytokinesis and required for the proper completion of abscission. *Mol. Biol. Cell* **24,** 2785–2794
63. Ali, A., Veeranki, S. N., and Tyagi, S. (2014) A SET-domain-independent role of WRAD complex in cell-cycle regulatory function of mixed lineage leukemia. *Nucleic Acids Res.* **42,** 7611–7624
64. Li, D. W., Yang, Q., Chen, J. T., Zhou, H., Liu, R. M., and Huang, X. T. (2005) Dynamic distribution of Ser-10 phosphorylated histone H3 in cytoplasm of MCF-7 and CHO cells during mitosis. *Cell Res.* **15,** 120–126
65. Zhou, H., Li, D., Song, L., Liu, R., Chen, J., and Huang, X. (2008) Thr11 phosphorylated H3 is associated with centromere DNA during mitosis in MCF-7 cells. *Mol. Cell. Biochem.* **311,** 45–50
66. Li, M. M., Nilsen, A., Shi, Y., Fusser, M., Ding, Y. H., Fu, Y., Liu, B., Niu, Y., Wu, Y. S., Huang, C. M., Olofsson, M., Jin, K. X., Lv, Y., Xu, X. Z., He, C., *et al.* (2013) ALKBH4-dependent demethylation of actin regulates actomyosin dynamics. *Nat. Commun.* **4,** 1832
67. Dharmarajan, V., Lee, J. H., Patel, A., Skalnik, D. G., and Cosgrove, M. S. (2012) Structural basis for WDR5 interaction (Win) motif recognition in human SET1 family histone methyltransferases. *J. Biol. Chem.* **287,** 27275–27289
68. Patel, A., Dharmarajan, V., and Cosgrove, M. S. (2008) Structure of WDR5 bound to mixed lineage leukemia protein-1 peptide. *J. Biol. Chem.* **283,** 32158–32161
69. Townsend, E. (2012) *Development of a Novel Inhibitor to the Conserved Developmental Regulator, WDR5, for Treatment of Acute Leukemia.* Ph.D. thesis, University of Michigan
70. Karatas, H., Townsend, E. C., Cao, F., Chen, Y., Bernard, D., Liu, L., Lei, M., Dou, Y., and Wang, S. (2013) High-affinity, small-molecule peptidomimetic inhibitors of MLL1/WDR5 protein-protein interaction. *J. Am. Chem. Soc.* **135,** 669–682
71. Trievel, R. C., and Shilatifard, A. (2009) WDR5, a complexed protein. *Nat. Struct. Mol. Biol.* **16,** 678–680
72. Dias, J., Van Nguyen, N., Georgiev, P., Gaub, A., Brettschneider, J., Cusack, S., Kadlec, J., and Akhtar, A. (2014) Structural analysis of the KANSL1/WDR5/KANSL2 complex reveals that WDR5 is required for efficient assembly and chromatin targeting of the NSL complex. *Genes Dev.* **28,** 929–942
73. Hale, B. G., Randall, R. E., Ortín, J., and Jackson, D. (2008) The multifunctional NS1 protein of influenza A viruses. *J. Gen. Virol.* **89,** 2359–2376
74. Qin, S., Liu, Y., Tempel, W., Eram, M. S., Bian, C., Liu, K., Senisterra, G., Crombet, L., Vedadi, M., and Min, J. (2014) Structural basis for histone mimicry and hijacking of host proteins by influenza virus protein NS1. *Nat. Commun.* **5,** 3952
75. Ernst, P., and Vakoc, C. R. (2012) WRAD: enabler of the SET1-family of H3K4 methyltransferases. *Brief Funct. Genomics* **11,** 217–226
76. Greer, E. L., and Shi, Y. (2012) Histone methylation: a dynamic mark in health, disease and inheritance. *Nat. Rev. Genet.* **13,** 343–357
77. Matthews, A. G., Kuo, A. J., Ramón-Maiques, S., Han, S., Champagne, K. S., Ivanov, D., Gallardo, M., Carney, D., Cheung, P., Ciccone, D. N., Walter, K. L., Utz, P. J., Shi, Y., Kutateladze, T. G., Yang, W., *et al.* (2007) RAG2 PHD finger couples histone H3 lysine 4 trimethylation with V(D)J recombination. *Nature* **450,** 1106–1110
78. Goldsworthy, M., Absalom, N. L., Schröter, D., Matthews, H. C., Bogani, D., Moir, L., Long, A., Church, C., Hugill, A., Anstee, Q. M., Goldin, R., Thursz, M., Hollfelder, F., and Cox, R. D. (2013) Mutations in Mll2, an H3K4 methyltransferase, result in insulin resistance and impaired glucose tolerance in mice. *PLoS One* **8,** e61870
79. Nakagawa, T., and Xiong, Y. (2011) X-linked mental retardation gene CUL4B targets ubiquitylation of H3K4 methyltransferase component WDR5 and regulates neuronal gene expression. *Mol. Cell* **43,** 381–391
80. Lim, D. A., Huang, Y. C., Swigut, T., Mirick, A. L., Garcia-Verdugo, J. M., Wysocka, J., Ernst, P., and Alvarez-Buylla, A. (2009) Chromatin remodelling factor Mll1 is essential for neurogenesis from postnatal neural stem cells. *Nature* **458,** 529–533
81. Ang, Y. S., Tsai, S. Y., Lee, D. F., Monk, J., Su, J., Ratnakumar, K., Ding, J., Ge, Y., Darr, H., Chang, B., Wang, J., Rendl, M., Bernstein, E., Schaniel, C., and Lemischka, I. R. (2011) Wdr5 mediates self-renewal and reprogramming via the embryonic stem cell core transcriptional network. *Cell* **145,** 183–197
82. Jiang, H., Shukla, A., Wang, X., Chen, W. Y., Bernstein, B. E., and Roeder, R. G. (2011) Role for Dpy-30 in ES cell-fate specification by regulation of H3K4 methylation within bivalent domains. *Cell* **144,** 513–525